PB-240 584

INTERFEROMETRIC INSTRUMENTATION FOR PARTICLE SIZE ANALYSIS

D. W. Roberds, et al

Arnold Engineering Development Center

Prepared for:

National Environmental Research Center

June 1974

DISTRIBUTED BY:

NTIS

National Technical Information Service
U. S. DEPARTMENT OF COMMERCE

090175

PB240589

EPA-650/2-73-034

June 1974

Environmental Protection Technology Series

[illegible] FOR PARTICLE SIZE ANALYSIS

PB 240 584

EPA-650/2-73-034

INTERFEROMETRIC INSTRUMENTATION FOR PARTICLE SIZE ANALYSIS

by

D.W. Roberds, W.M. Farmer, and A.E. Lennert

Arnold Research Organization, Inc.
Arnold Air Force Station, Tennessee 37389

Interagency Agreement No. EPA-IAG-0177(D)
Program Element No. 1AA010
ROAP No. 26AAM

EPA Project Officer: John W. Davis

Chemistry and Physics Laboratory
National Environmental Research Center
Research Triangle Park, North Carolina 27711

Prepared for

OFFICE OF RESEARCH AND DEVELOPMENT
U.S. ENVIRONMENTAL PROTECTION AGENCY
WASHINGTON, D.C. 20460

June 1974

This report has been reviewed by the Environmental Protection Agency and approved for publication. Approval does not signify that the contents necessarily reflect the views and policies of the Agency, nor does mention of trade names or commercial products constitute endorsement or recommendation for use.

ABSTRACT

This report summarizes the results of a research program conducted to determine the characteristics and potential capabilities of particle size analysis using laser interferometer techniques. Theoretical and experimental analyses are reported which indicate that a range of particle sizes from submicron to millimeters in diameter can be determined when the cross-sectional shape of the particle is known. It is shown that number density can be determined from the interferometric measurements in certain restricted applications. The limitations and potentialities of this method of determining particle size are discussed in detail.

CONTENTS

		Page
1.0	INTRODUCTION	7
2.0	THEORETICAL INTERFEROMETRIC PARTICLE SIZE ANALYSIS	
	2.1 General	8
	2.2 Single Particle Visibility Determination	11
	2.3 Determination of Number Density from Visibility Measurements	19
	2.4 Error Analysis	
	2.4.1 Error Analysis for Spherical Particles	20
	2.4.2 Error Analysis for Long Narrow Cylinders	23
	2.5 Visibility for Non-Paraxial Observations of Particles with Sizes Much Greater than a Wavelength	25
3.0	EXPERIMENTAL OBSERVATIONS	
	3.1 Experimental Evaluation	27
	3.2 Large Particle Error Analysis	30
	3.3 Experimental Results of Large Particle Observations	33
	3.4 Experimental Results of Small Particle Observations	43
4.0	ELECTRONIC INSTRUMENTATION	
	4.1 General	47
	4.2 Visibility from Peak Values	47
	4.3 Continuous Measurement of Signal Visibility	48
5.0	SUMMARY AND CONCLUSIONS	
	5.1 Passage Angles of the Particle through the Interference Fringes	49
	5.2 Relative Beam Intensities Used to Form the Interference Fringes	50
	5.3 Relative Coherence of the Beams	50
	5.4 Photon-Limited Signals	50
	5.5 Radiation Pressure Effects on Very Small Particles	50
	5.6 Light Absorption by the Particles	50
	5.7 Index of Refraction of Medium Surrounding the Particles	51
	5.8 Limiting Particle Size (Maximum and Minimum)	51
	5.9 Particle Shape Effects	52
	5.10 Multiple Particle Signals	53
6.0	RECOMMENDATIONS	53
	REFERENCES	54

Preceding page blank

ILLUSTRATIONS

Figure		Page
1.	Generation of Free Space Interference Fringes with a Laser Doppler Velocimeter System	9
2.	Fringe Intensity Distribution in y-z Plane	10
3.	Signal Waveforms	13
4.	Visibility Functions Near Geometric Center as a Function of D/δ and $L \sin(\beta)/\delta$	15
5.	Range of the Unambiguous Determination of Particle Size as a Function of Angle Between the Illumination Beams	17
6.	Example of a Multi-Beam Interferometer Arrangement and the Different Observational Modes	18
7.	Signal Visibility as a Function of Number of Observable Particles	21
8.	Maximum Observable Particle Density as a Function of Particle Diameter for a Visibility of 0.01 and an Illuminating Wavelength of 0.5 μm	22
9.	Uncertainty Curve for a Spherical Particle with Size Determined by a Visibility Measurement	24
10.	Uncertainty Curve for a Long Narrow Cylinder with Size Determined by a Visibility Measurement	25
11.	Visibility for Non-Paraxial Observation of a Large Particle Compared to Illuminating Wavelength λ_o	26
12.	Schematic of the Optical Arrangement for the Experiment Observations	27
13.	Photograph of Path Compensating Beam Splitting Blocks.	28
14.	Schematic of the Two-Dimensional Bragg Cell Arrangement	28
15.	Photograph of the Overall Optical System	29
16.	Photograph of the Particle Holder and Traverse System	31
17.	Schematic of the Data Reduction System	32
18.	Experimental and Theoretical Illuminating Intensity Distribution in the Probe Volume	34

Figure		Page
19.	Experimental and Theoretical Comparison for a Long Narrow Cylinder at Different Orientation Angles	35
20.	Comparison of Theoretical and Experimental Paraxial Visibility for a Spherical Particle.	37
21.	Average Signal Visibility as a Function of Particle Trajectory for Different D/δ	38
22.	Variation of Visibility for Different D/δ and Solid Collection Angle	39
23.	Comparison of Number Density Measurements by Image Computer with Those Made By an Interferometer	41
24.	Photograph of Interferometer Signal versus Time as the Number of Particles Passing through the Probe Volume Changes	42
25.	Experimental Arrangement for Small Particle Observation	44
26.	Relative Particle Size Distribution of Laboratory Particles.	45
27.	Particle Visibility Histogram for Laboratory Air Particles.	46
28.	Electronics for Visibility Measurement from Peak Values	47
29.	Electronics for Continuous Measurement of Visibility	48

1.0 INTRODUCTION

Numerous techniques exist to determine the size of small particles (Ref. 1). Optical techniques which allow visible analysis of the particle represent the most accurate means available for size determination. These techniques range in diversity from simple microscope measurements to the more sophisticated methods of size determination from scattered light measurements. Each optical technique has its own peculiar limitation for the determination of particle size. For example, microscope analysis usually requires that the particles be stationary, and that the size of the particles be greater than several wavelengths of the light illuminating it. On the other hand, light scattering measurements which can determine particle size less than a wavelength in diameter require á priori knowledge of particle shape, index of refraction, and in some cases, the absolute values of the scattered light intensity must be measured accurately. Holographic techniques have been used extensively in the measurement of particle sizes in a number of different applications (Refs. 2, 3, and 4). Holographic measurements offer the advantage of extreme depths of field; however, the resolutions are limited by the velocity of the dynamic particles (Refs. 2 and 3). Furthermore, since holography does not as yet provide on-line measurements, the analysis of particle hologram images is somewhat tedious and time consuming. Thus, a need exists for a device that can rapidly determine particle sizes lower than the resolution limit of standard microscope systems and that is not restricted to measuring stationary particles.

The purpose of this report is to describe the research performed to develop a technique and corresponding instrumentation to satisfy the above needs. The results of both the analytical and experimental work indicate the feasibility of using interferometric techniques for measuring particle sizes. The characteristics and limitations of a prototype instrument are summarized. Predicted upon the results, recommendations for continued effort are made to develop a viable instrument for on-line particle size measurements.

Preceding page blank

2.0 THEORETICAL INTERFEROMETRIC PARTICLE SIZE ANALYSIS

2.1 GENERAL

In this section, a review of the theory and analysis of the interferometric particle sizing technique will be discussed. Figure 1 illustrates that when two coherent laser beams (assumed to be in the TEM_{oo} mode) are brought to a simultaneous cross-focus region by means of a lens, interference fringes are formed. In the region of focus, the wavefronts are planar and tilted relative to each other according to the included angle, α, between the beams. Propagation vectors are $\vec{K}_o$ and $\vec{K}_2$. The interference fringes generated are planes parallel to the bisector between the beams and perpendicular to the plane of the beams. The distance between successive fringes, δ, is given by

$$\delta = \frac{\lambda_o}{2\eta \sin \alpha/2} \tag{1}$$

where η is the index of refraction of the medium surrounding the particle and λ_o is the wavelength of the interfering light. A particle traversing a set of interference fringes will receive varying amounts of illumination as it passes alternately through the bright and dark regions. If the light scattered by the moving particle is focused onto a photomultiplier (PM) tube, as shown in Fig. 1, the velocity of the particle normal to the interference fringes may be determined from the time elapsed between successive peaks in the collected light intensity (Refs. 5, 6, and 7). Furthermore, particle size information is also inherent in the collected scattered light signal (Refs. 8 and 9).

Define a coordinate system (Fig. 1) such that the z axis lies along the bisector of the beams, x is the direction of polarization, and y is orthogonal to both x and z. Let the electric field amplitudes E_1 and E_2 of the two laser beams be expressed as

$$E_1 = E_o \exp\left(-\frac{x_1^2 + y_1^2}{b_o^2}\right) \exp\left(i\omega t - ikz_1 + i\phi_1\right)$$

$$E_2 = E_o \exp\left(-\frac{x_2^2 + y_2^2}{b_o^2}\right) \exp\left(i\omega t - ikz_2 + i\phi_2\right) \tag{2}$$

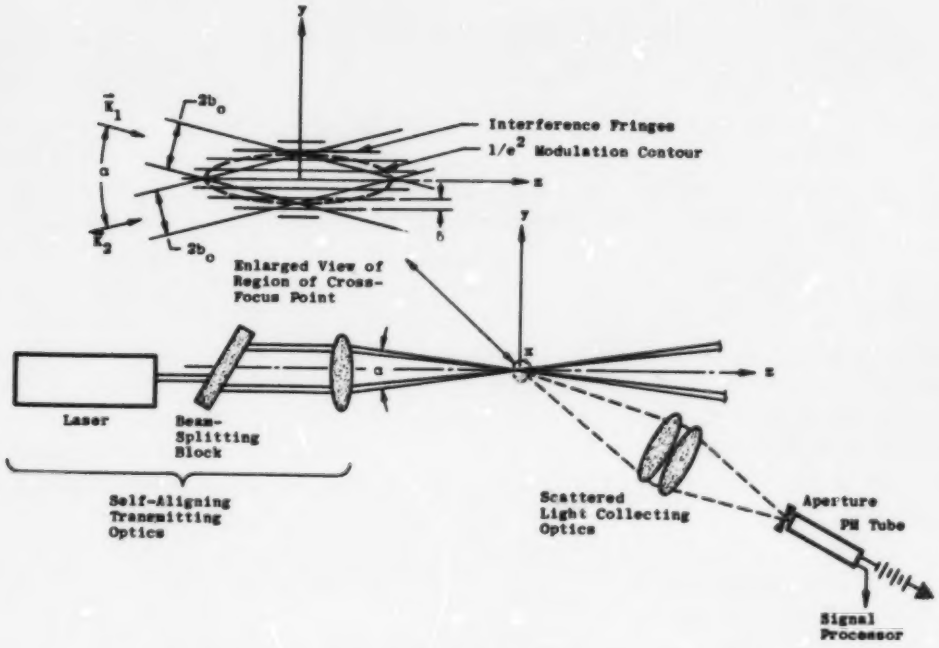

Figure 1. Generation of free space interference fringes with a laser doppler velocimeter system.

Each electric field is expressed in terms of its own coordinate system referred to its own direction of propagation: z_i is in the direction of propagation of the ith beam, x_i is in the direction of polarization, and y_i is orthogonal to the $x_i z_i$ plane. The origin of both coordinate systems is located at the cross-focus of the two beams. In these equations, E_o is the field on the centerline of each beam, ω is the optical frequency, t is time, $k = 2\pi/\lambda$, where λ is the laser wavelength, and ϕ_1, ϕ_2 are arbitrary phase factors. Since the beams are polarized in the same direction, $x_1 = x_2 = x$ and assume $\phi_1 = \phi_2$. The variable $b_o = 2f_L\lambda/\pi d_b$ is the radial distance at which the field amplitude of that beam has fallen off to e^{-1} times its value on centerline; the amplitude falls off in a Gaussian manner with radial distance = $(x_i^2 + y_i^2)^{1/2}$. The variable f_L is the focal length of the beam focusing lens and d_b is the diameter of the input laser beam.

The two plane wave radiations interfere to form a high contrast fringe system. By summing E_1 and E_2 of Eq. (2) and transforming coordinates to the symmetrically located coordinates xyz, the intensity I_o in the cross-over region can be expressed as (Ref. 9)

$$I_o = \frac{2E_o^2}{Z'} \exp\left[-\frac{2}{b_o^2}\left(x^2 + y^2\cos^2\frac{\alpha}{2} + z^2\sin^2\frac{\alpha}{2}\right)\right]\left[\cosh\left(\frac{2}{b_o^2}\right)yz\sin\alpha + \cos\left(\frac{2\pi y}{\delta}\right)\right] \quad (3)$$

where z' is the impedance of the surrounding medium.

Equation (3) shows the only dependence on x is the factor exp $[-2x^2/b_o^2]$; therefore, the intensity distribution does not vary in the x direction except to decrease in a Gaussian manner. Figure 2 is a sketch of Eq. (3) for the plane x = 0 (y-z plane). The fringes extend parallel to the z axis. For z = 0 the cosh term is unity for all y, and the distribution consists of alternate bright and dark fringes decreasing in intensity in a Gaussian manner in the y direction. Farther out on the z axis, beyond the cross-over point of the beams, the cosh term becomes significant before the Gaussian fall off causes the intensity to go to zero. One can visualize from Fig. 2 the two beams separating from each other beyond the cross point.

A "probe volume" can be defined from Eq. (3) as that surface where the Gaussian factor

$$\exp\left[-\frac{2}{b_o^2}\left(x^2 + y^2\cos^2\frac{\alpha}{2} + z^2\sin^2\frac{\alpha}{2}\right)\right]$$

has decreased to e^{-2}. Setting y = z = 0, the point where this surface

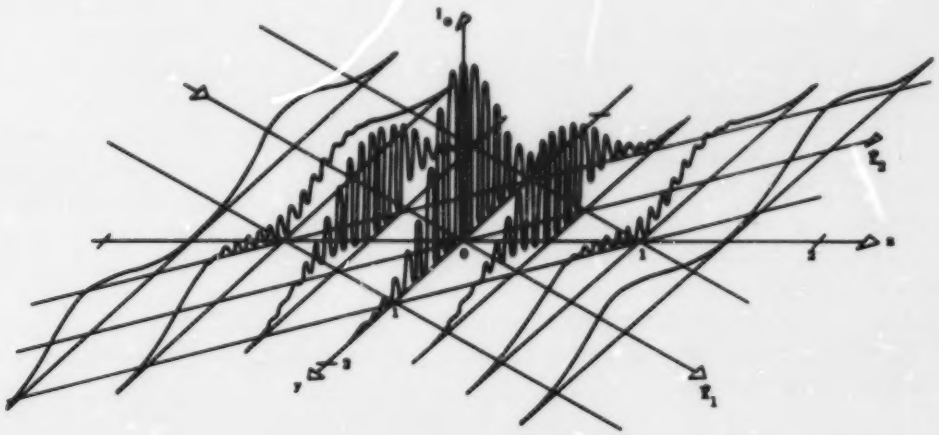

Figure 2. Fringe intensity distribution in y-z plane.

intersects the x axis is found as

$$\exp\left(-\frac{2}{b_o^2}x^2\right) = e^{-2}$$

$$x = b_o$$

Similarly, the y and z axis intersections are

$$y = b_o/\cos(\alpha/2)$$

$$z = b_o/\sin(\alpha/2)$$

Note that for beam separation angle α small, the probe volume is cigar-shaped, extending considerably farther in the z direction than in either the x or y directions.

A photomultiplier tube shown in Fig. 1 is used to detect the light signal scattered from a particle which passes through the fringe system. It is important to note that the collected light intensity, even from a point particle, may not be proportional to the illuminating intensity in the probe volume. This is because light from each beam is scattered by the particle in lobes independently of that from the other beam. The general case of the light scattered from a single particle illuminated by two beams has been reported (Ref. 9) using the relationships of light scattered from a spherical particle immersed in a dielectric medium scattering plane waves (Ref. 10). It can be shown that where the two illuminating beams are polarized in the same direction, there are two different conditions under which the collected light scattered from a point particle will in fact be proportional to the light incident on the particle. These conditions, either of which may be met, are:

1. The beam separation angle α is small, and the light is collected from any point in the y-z plane.
2. The light is collected paraxially, i.e., from a point near the z axis (regardless of the value of α). In the following development one of these conditions is assumed to be met.

2.2 SINGLE PARTICLE VISIBILITY DETERMINATION

Suppose a particle whose dimensions are very small compared to the fringe spacing passes through the probe volume. The detected light intensity will then trace out the illuminating intensity I_o in the probe

volume. For example, if a point particle moves along the y axis the signal, as viewed on an oscilloscope connected to the PM tube, will trace out the center waveform depicted in Fig. 2 (similar also to Fig. 3b). Here the signal alternately builds up as the scatterer crosses a bright fringe then falls to zero as the scatterer passes through a dark fringe. The peak intensity crossing the bright fringes increases as the particle approaches the center of the fringe set then decreases as the particle leaves.

Now suppose the particle is not very small compared to a fringe spacing. The particle cannot be completely hidden in a dark fringe because its size will partially overlap the two adjoining bright fringes. A larger particle following the same path as the point particle might produce the signal shown in Fig. 3a. Here the scattered intensity does not fall all the way to zero between bright fringes because the particle is always intercepting some light. A still larger particle, overlapping yet more of the adjoining fringes during its traversal, might produce a signal similar to that of Fig. 3c. These figures show that the magnitude of oscillation of the signal decreases with increase in particle size. In fact, for certain particle dimensions comparable to the fringe spacing the PM tube signal may display only a Gaussian form with no superimposed oscillation. Theoretical analysis verifies this result.

To show the dependence of the shape of the signal on size, it is assumed (Ref. 9) that a simple average of the illuminating intensity over the cross-sectional area of the particle can be used to find the mean incident intensity. That is, the scattered intensity I_s is assumed to be proportional to (again, with the light collected paraxially)

$$I_s \sim \frac{1}{A_p} \iint_{A_p} I_o \, dx \, dy \tag{4}$$

where A_p is the cross-sectional particle area. Actual measurements of known particle sizes show good agreement with theory developed from this assumption, and it will be used in what follows.

The integration of I_o given by Eq. (3) over a surface area is not easily obtained. However, if certain simplifying assumptions are made, closed form solutions can be found for the cross-sectional areas of spheres and cylinders. Assume the maximum particle dimension is small compared to b_o. This allows one to assume that the slowly varying exponential and cosh terms remain constant over the scatterer

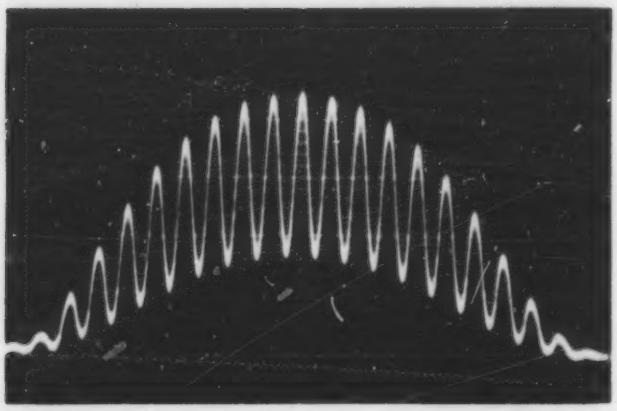

a. Visibility = 0.47

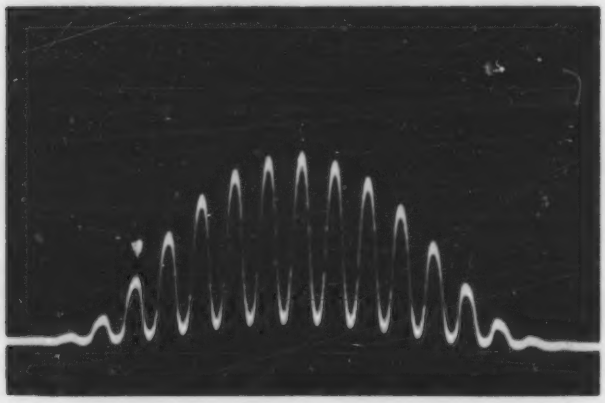

b. Visibility = 0.89

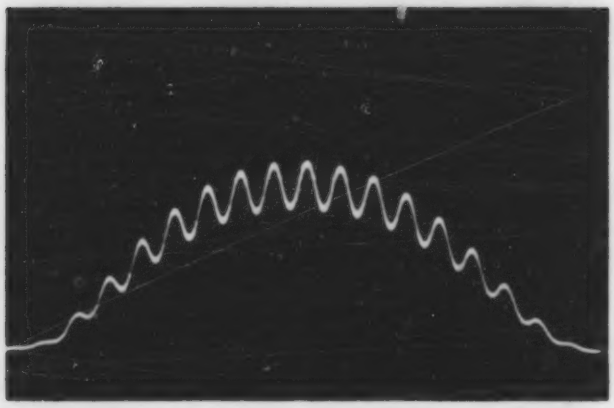

c. Visibility = 0.17

Figure 3. Signal waveforms.

surface. The condition that the dimension D be small compared to b_o has been shown to be met if (Ref. 11)

$$\delta \leq 5\, b_o \tag{5a}$$

$$D \leq \delta \tag{5b}$$

Integration then gives, for the cross section of a sphere,

$$I_s \sim \exp\left[-\frac{2}{b_o^2}\left(x^2 + y^2 \cos^2\frac{\alpha}{2} + z^2 \sin^2\frac{\alpha}{2}\right)\right] \times \left\{\cosh\left[\frac{2}{b_o^2}\, yz \sin\alpha\right] + \left[\frac{2J_1(\pi D/\delta)}{(\pi D/\delta)}\right] \cos\left[\frac{2\pi y}{\delta}\right]\right\} \tag{6}$$

Here x, y, and z refer to the coordinates of the center of the spherical scatterer, D is the sphere diameter, and J_1 is a first-order Bessel function of the first kind.

Equation (6) is an expression for the scattered light collected paraxially from a spherical particle of diameter D located at point x, y, z. It shows dependence of the signal shape on the diameter. If a particle follows some trajectory through the fringe set and the signal is displayed on an oscilloscope screen, the result might look like any of those included in Fig. 3. This type of signal will depend on the ratio of the particle diameter to the fringe spacing. Note that there must be some component of velocity in the y direction in order for the oscillating cosine term to be displayed.

Equation (6) may be considered as the sum of a Gaussian modulated cosh function, known as the "pedestal" or "d-c" component, and a Gaussian modulated cosine known as the "a-c" component of the signal. The ratio of the a-c magnitude to the pedestal is a measure of how "visibile" the a-c component is and is called the "visibility", where

$$V \triangleq \frac{\text{a-c magnitude}}{\text{pedestal}} = \frac{\left[\frac{2J_1(\pi D/\delta)}{\pi D/\delta}\right]}{\cosh\left(\frac{2yz}{b_o^2}\sin\alpha\right)} \tag{7}$$

when either the plane z = 0 or y = 0, the cosh term is unity and the visibility reduces to the numerator of Eq. (7). In either of these planes, the visibility is then only a function of particle size, i.e.,

$$V = \frac{2J_1(\pi D/\delta)}{(\pi D/\delta)} \qquad (y = 0 \text{ or } z = 0) \tag{8}$$

A similar derivation for a cylindrically shaped particle gives for the visibility in the y = 0 or z = 0 plane:

$$V = \text{sinc}\,(L/\delta \sin\beta) \quad \text{sinc}\,(D/\delta \cos\beta) \tag{9}$$

where the function sinc (u) is defined as $\sin(\pi u)/\pi u$, L is the length of the cylinder, D its diameter, and β is the angle the major axis of the cylinder makes with the fringe planes. The major axis is assumed to be in a plane normal to the fringe planes.

Under the further assumption that the cylinder diameter $D \ll \delta$, then Eq. (9) reduces to

$$V \cong \text{sinc}\,(L/\delta \sin\beta) \tag{10}$$

The visibility functions, Eqs. (8) and (10), are plotted in Fig. 4. Examination of these equations and the curves of Fig. 4 show that the

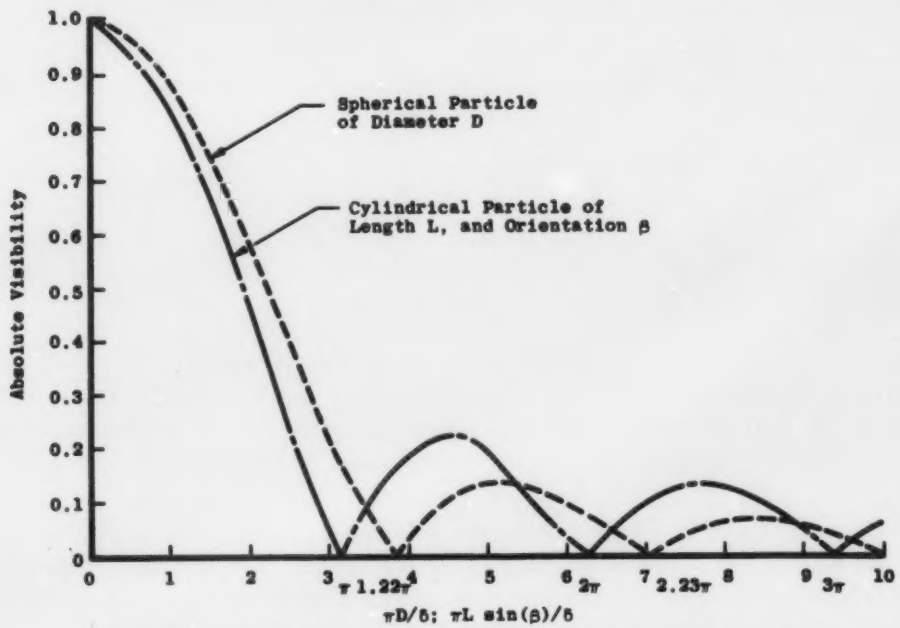

Figure 4. Visibility functions near geometric center as a function of D/δ and L sin (β)/δ.

visibility has zeros; i.e., for certain particle dimensions, no a-c term will appear. In addition, when the visibility function is less than about 0.17 for spheres and about 0.24 for cylinders, different particle sizes can have the same value of visibility. In addition, the visibility function changes sign as it passes through successive zeros. Negative visibility means that more light is scattered when the particle is centered over a dark fringe (and overlapping adjacent bright fringes) than when it is centered over a bright fringe (and overlapping adjacent dark fringes). There is no way in practice to quickly determine if a small measured visibility is positive or negative; therefore, only the absolute value of the visibility is plotted in Fig. 4. If the visibility can be determined within an accuracy of one per cent, Fig. 4 shows that spherical particle diameters can be determined unambiguously over the size range $0.1 < D/\delta < 1.0$

When the particle passes through the probe volume the oscilloscope signal may be photographed, and the ratio of the ac to the pedestal may be directly measured from the waveform. Under the conditions that the particle was moving in the "y" direction (to display the cosine term) and that the fringe spacing is small compared to b_o (such that a number of cycles are included in the waveform) the visibility can be obtained using the Michelson visibility definition (Ref. 12):

$$V = \frac{I_{max} - I_{min}}{I_{max} + I_{min}} \tag{11}$$

where I_{max} is the intensity of light scattered when the particle is centered in a bright fringe and I_{min} is the intensity scattered when the particle is centered in the adjoining dark fringe. Obviously, measuring the fringe visibility using oscilloscope photographs and the above analysis is time consuming.

As an alternative method of measuring the visibility, the a-c component may be separated from the lower frequency pedestal by electronic filtering. The two components can then be determined separately and then combined in an analog divider to acquire the visibility.

Visibility measurements should be made when the particle is either in the $y = 0$ or $z = 0$ plane (x-z plane or x-y plane). Particles will generally be flowing in the "y" direction, and one possible technique that can be used to ensure that the particles are near the $z = 0$

condition when the measurement is made by optical aperturing. As will be shown in a later section, for a particle moving within a region near z = 0 there is little variation in the visibility. Optically aperturing the system so that particles outside the specified range are not "seen" by the collection optics would ensure valid visibility measurements. It may also be possible to electronically aperture the system, as discussed in Section 4.3.

Consider the size resolution of visibility measurements in terms of classical lens resolution limits. If two parallel beams are separated by 0.8 lens diameters before they are focused to the probe volume, the interference fringe spacing is just equal to the Rayleigh resolution limit of the lens (Ref. 10). If the visibility measurements satisfy the above resolution limits then particle sizes may be determined that are approximately ten times smaller than the resolution limit of the transmitting optics. Figure 5 indicates the particle size range which can be determined for the above criteria as a function of the angle between the interfering beams. The upper curve describes

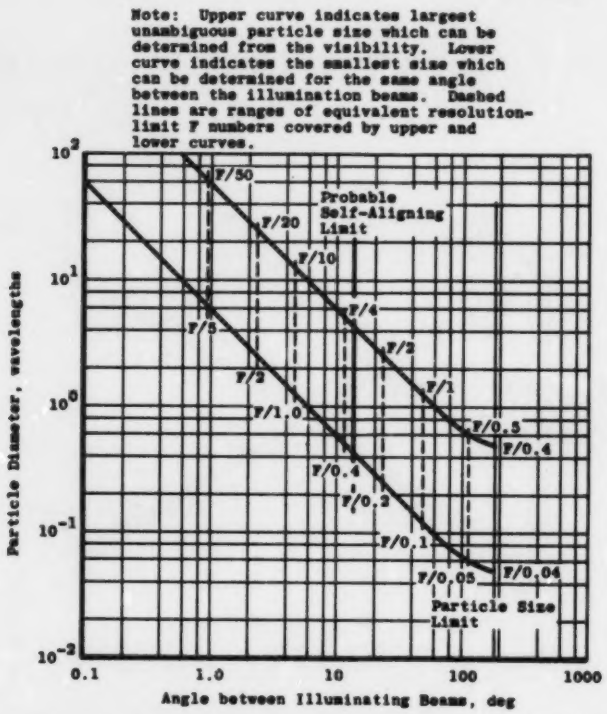

Figure 5. Range of the unambiguous determination of particle size as a function of angle between the illumination beams.

the upper size limit, while the lower curve describes the lower size limit. The dashed vertical lines indicate the range of f numbers required for lenses to resolve a particle of the same size. The largest possible included angle between the beams is 180°, which yields a fringe spacing of $\lambda/2$. Thus, the smallest possible size that can be measured by this technique is $\lambda/20$.

In Fig. 5 there is a vertical solid line labeled "probable self-aligning limit." This limit arises because a single lens cannot accurately focus and cross two beams for included angles greater than approximately 12°, which corresponds to a transmitting lens f number of approximately 4. For angles greater than 12° an optical arrangement similar to that shown in Fig. 6 is required. In this arrangement a lens is used to focus the beams, and mirrors cross the beams at some predetermined position. Since the point of intersection is an independent variable, with respect to the focusing lens, such systems are not self-aligning. Such optical systems are extremely sensitive to vibration and the precise alignment requirements for the beams to acquire high quality interference fringes is difficult to attain.

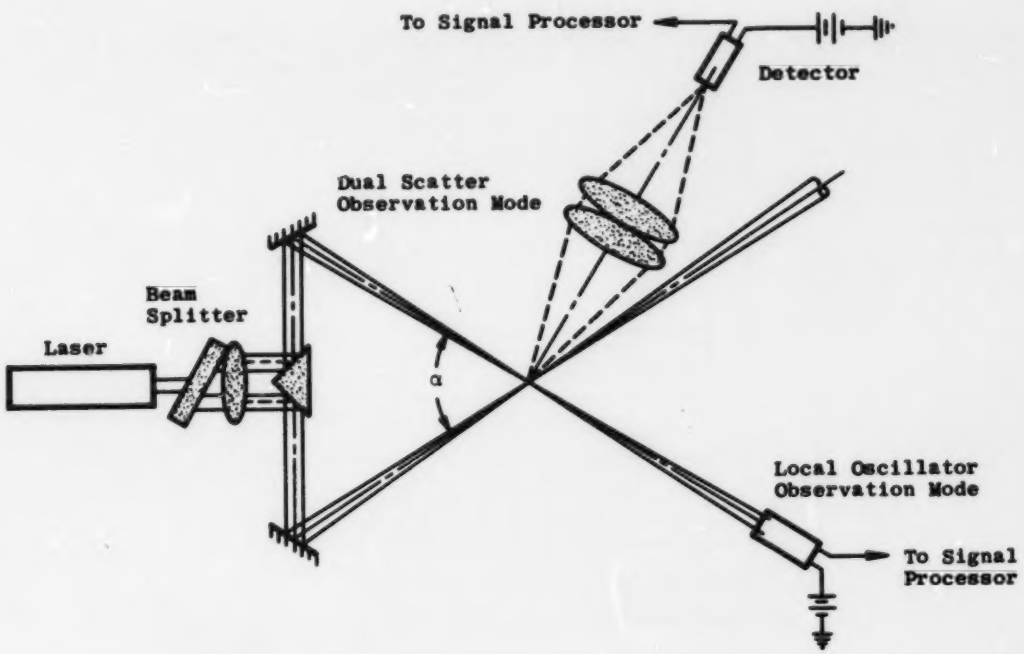

Figure 6. Example of a multi-beam interferometer arrangement and the different observational modes.

In reviewing the important criteria for the determination of particle sizes from visibility measurements it is found that:

1. The two illuminating beams should be of the same center-line intensity and polarized in the same direction.
2. The observations should be made paraxially.
3. The particle trajectory should not depart greatly from the x-y plane (z = 0).
4. The maximum dimension of the particle should be relatively small compared with the probe volume width in order that the low frequency variation of the "pedestal" can be neglected when averaging the incident intensity over the surface of the particle.

2.3 DETERMINATION OF NUMBER DENSITY FROM VISIBILITY MEASUREMENTS

The number density of particles, when many particles simultaneously occupy the probe volume, can also be determined from visibility measurements. The visibility may be written (Ref. 9) as

$$V = \frac{\langle P_s^1 \rangle}{\langle P_d^1 \rangle} \tag{12}$$

where p_s^1 represents the a-c signal power for a single particle detected by the collection optics and p_d^1 represents the pedestal, or d-c signal power for the same particle, and the time average is taken over one complete cycle of information. The visibility function as defined by Eq. (12) is independent of the absolute value of the scattering properties of the particle and is solely dependent upon relative values. Thus, particle sizing by this technique requires only a single measurement, at a fixed angle, of the relative scattering intensity between dark and bright fringes, and not a pair of measurements at different angles as would be required by the usual process of determining sizes from light intensity measurements and the Mie theory.

Analogous to Eq. (12), the visibility function for N particles in the probe volume is defined as

$$\bar{V}_N = \frac{\langle \bar{P}_S^N \rangle}{\langle \bar{P}_d^N \rangle} \tag{13}$$

where $\bar{P}_S^N$ and $\bar{P}_d^N$ are the respective a-c and d-c signal power collected for N particles in the focal volume. It has been shown (Ref. 13) that

$$\langle \bar{P}_S^N \rangle = \sqrt{N} \langle \bar{P}_S^1 \rangle \tag{14}$$

$$\langle \bar{P}_d^N \rangle = N \langle \bar{P}_d \rangle \tag{15}$$

Combining Eqs. (14), (15), and (12) the following is obtained:

$$V_N = \frac{\bar{V}}{\sqrt{N}} \tag{16}$$

where $\bar{V}$ is the ensemble average one particle visibility function for the size distribution of N particles. Thus, from Eq. (16) N can be determined experimentally by adjusting the fringe spacing δ until $\bar{V}$ is constant, i.e., approximately unity for the size distribution. Under this condition, the visibility measurement can reflect only the number of particles contributing to the signal: $\bar{V}_N \simeq 1/\sqrt{N}$ $(D \ll \delta)$ when a distribution of sizes for the N particles exists then there is, at present, no straight-forward procedure to determine the number of particles as a function of size from the visibility measurement. In Fig. 7 the visibility is plotted as a function of the number of detectable particles. Under the assumption that the visibility can be determined with an accuracy of one percent, Fig. 8 shows the limiting number density as a function of particle size that can be determined from visibility measurements, under the constraints that $D < \delta < 5b_o$. Figure 8 was obtained under the further condition that the diameter of the probe volume is determined solely by the e^{-2} intensity contour.

2.4 ERROR ANALYSIS

In this section a brief analysis is performed to determine the type of errors which can be expected in attempting to determine the particle size from a visibility measurement. Only errors associated with the measurement of spherical and cylindrical particle sizes will be discussed.

2.4.1 Error Analysis for Spherical Particles

Following a typical analysis (Ref. 17), the deviation in the visibility, ΔV, is

$$\Delta V = \frac{\partial V}{\partial D} \Delta D + \frac{\partial V}{\partial \delta} \Delta \delta \tag{17}$$

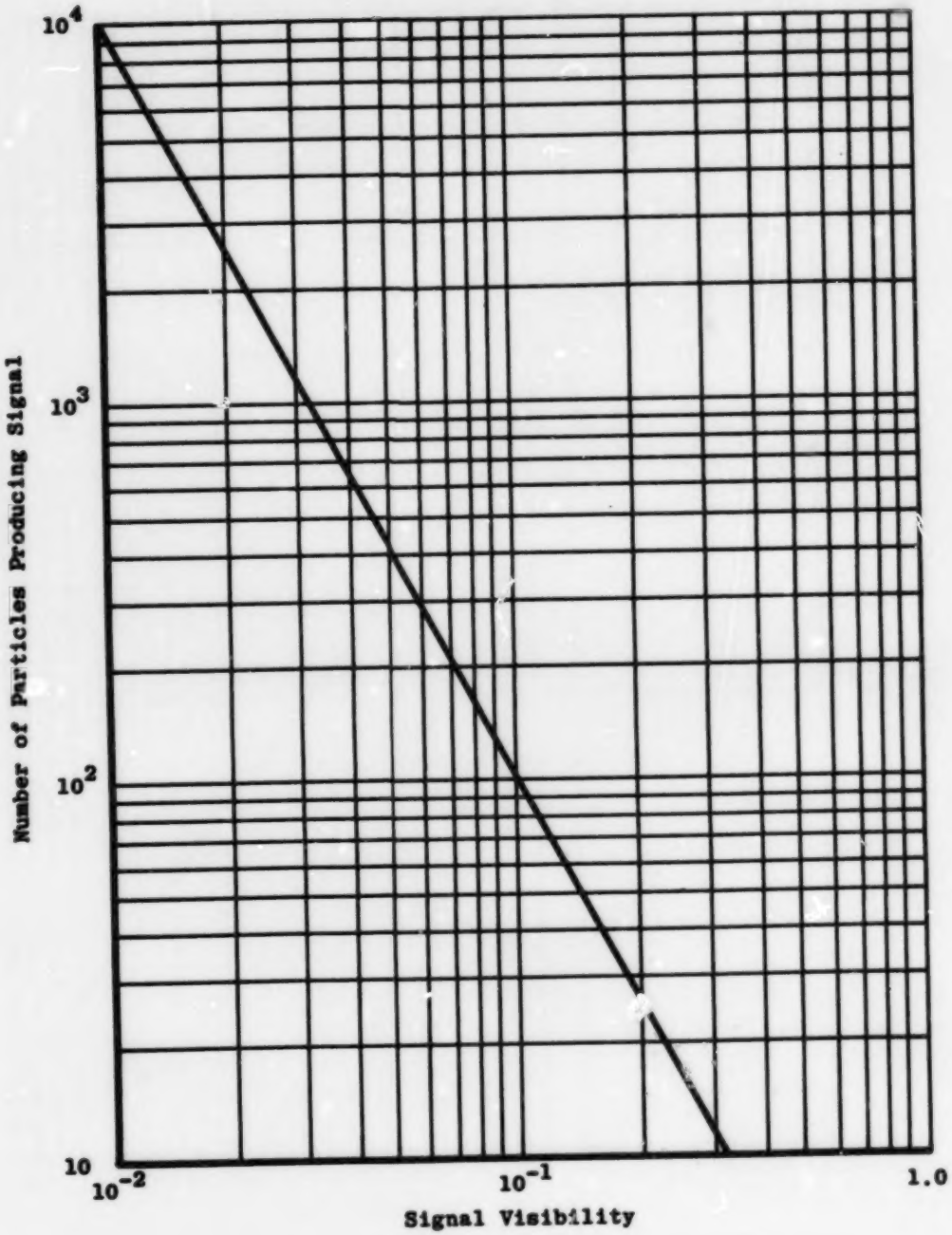

Figure 7. Signal visibility as a function of number of observable particles.

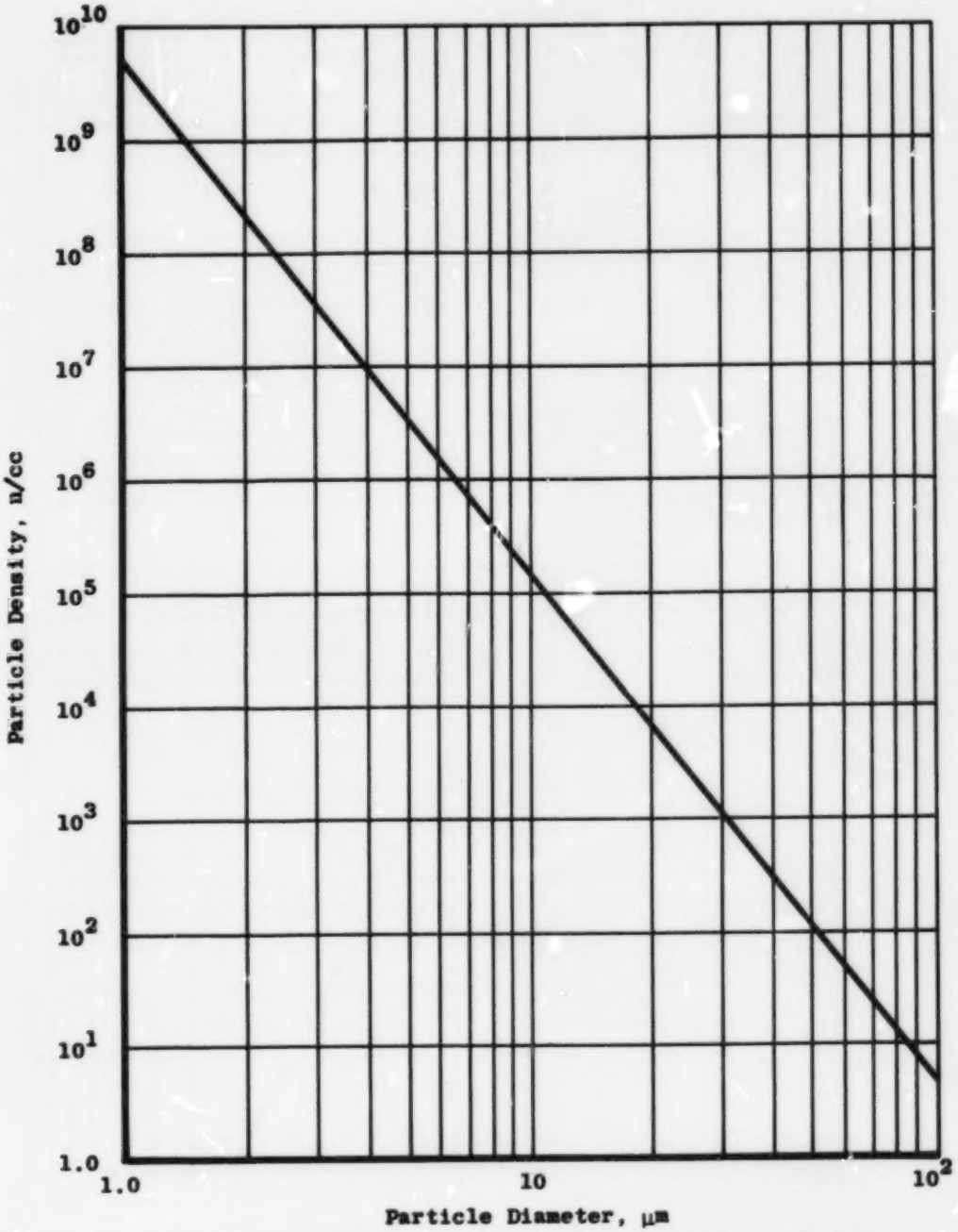

Figure 8. Maximum observable particle density as a function of particle diameter for a visibility of 0.01 and an illuminating wavelength of 0.5 μm.

Using Eq. (8) and standard Bessel function identities, Eq. (17) can be written as

$$\Delta V = -2J_2(\pi D/\delta)\Delta D/D + 2J_2(\pi D/\delta)\Delta\delta/\delta \tag{18}$$

where J_2 is a second-order Bessel function of the first kind. On solving Eq. (18) for $\Delta D/D$, the error estimate becomes

$$\Delta D/D = \frac{-\Delta V}{2J_2(\pi D/\delta)} + \frac{\Delta\delta}{\delta} \tag{19}$$

Thus the standard deviation, assuming no correlation between ΔV and $\Delta\delta$, is

$$\overline{\Delta D}/D = \pm\left[\frac{\overline{\Delta V}^2}{4J_2^2(\pi D/\delta)} + \frac{\overline{\Delta\delta}^2}{\delta^2}\right]^{1/2} \tag{20}$$

In terms of the experimental parameter, α(λ_o assumed constant), $\Delta\delta$ is given by:

$$\Delta\delta = -\lambda_o \csc(\alpha/2)\cot(\alpha/2)\Delta\alpha/4 \tag{21}$$

Figure 9 contains plots of Eq. (20) under the assumption that $\overline{\Delta\delta}^2$ is zero. The least uncertainty in the size measurement occurs for D/δ approximately in the range from 0.6 to 1.0. Here, small uncertainties in the diameter result from a given uncertainty in the visibility. The region of D/δ shown in Fig. 9 where uncertainties in diameter are high for a given visibility measurement can also be seen simply by looking at Fig. 4; where the curves of Fig. 4 approach the horizontal, a small error in measuring the visibility can result in a large error in D/δ.

2.4.2 Error Analysis for Long Narrow Cylinders

An estimate of the error to be expected for the size determination of long narrow cylinders ($D \ll \delta$) of arbitrary orientation will be discussed. As with the spherical particles, the deviation in V can be written as

$$\Delta V = \frac{\partial V}{\partial\beta}\Delta\beta + \frac{\partial V}{\partial\delta}\Delta\delta + \frac{\partial V}{\partial L}\Delta L \tag{22}$$

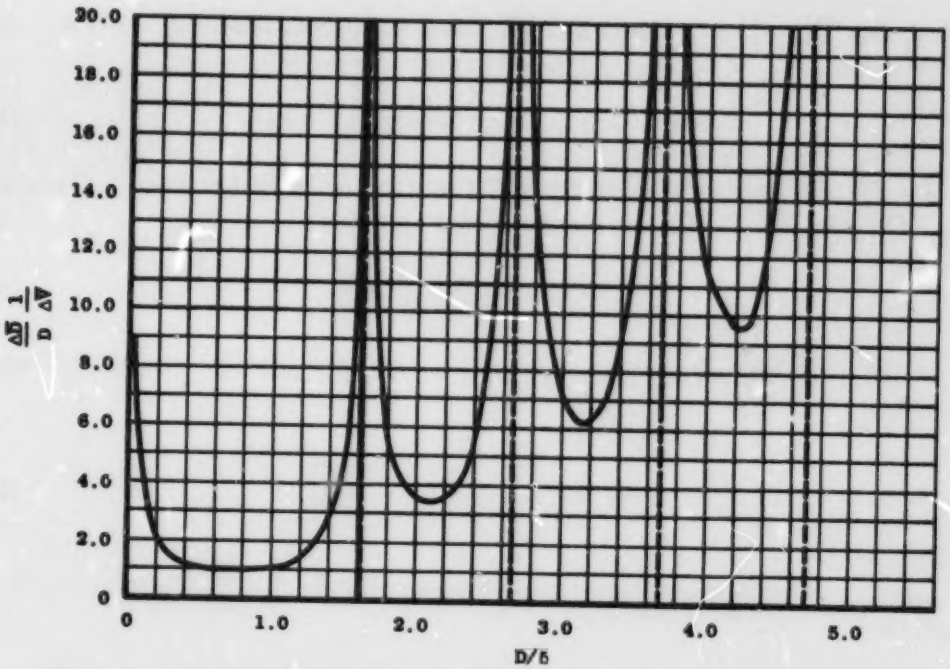

Figure 9. Uncertainty curve for a spherical particle with size determined by a visibility measurement.

Using Eq. (9) under the conditions imposed above gives the following values for the derivatives:

$$\frac{\partial V}{\partial \beta} = \cot(\beta)\left[\cos\left(\frac{\pi L}{\delta}\sin\beta\right) - V\right] \tag{23a}$$

$$\frac{\partial V}{\partial \delta} = -\left[\cos\left(\frac{\pi L}{\delta}\sin\beta\right) - V\right]/\delta \tag{23b}$$

$$\frac{\partial V}{\partial L} = \left[\cos\left(\frac{\pi L}{\delta}\sin\beta\right) - V\right]/L \tag{23c}$$

Solving Eq. (22) for $\Delta L/L$ by substituting Eqs. (23a), (23b), and (23c) gives

$$\Delta L/L = \frac{\Delta\delta}{\delta} - \Delta\beta\cot\beta + \Delta V/\left[\cos\left(\frac{\pi L}{\delta}\sin\beta\right) - V\right] \tag{24}$$

The standard deviation follows immediately as

$$\Delta\overline{L}/L = \pm\left\{\frac{\Delta\overline{\delta}^2}{\delta^2} + \Delta\overline{\beta}^2\cot^2\beta + \frac{\Delta\overline{V}^2}{\left[\cos\left(\frac{\pi L}{\delta}\sin\beta\right) - V\right]^2}\right\}^{1/2} \tag{25}$$

Equation (25) is plotted in Fig. 10 under the assumptions that $\Delta\beta$ and $\Delta\delta \simeq 0$. Trends in error propagation are seen that are similar to the spherical particle uncertainty curve (Fig. 9). The most important point to observe in the spherical particle case is that the least error possible lies between $V \simeq 1$ and the first zero (Fig. 4). Thus, not only does size determination become ambiguous when the particle size is greater than δ, but the uncertainty quickly increases. On the other hand, the uncertainty curve for the cylinder shows that regions exist after the first zero which also give as good a minimum error as was possible for $L \sin(\beta)/\delta < 1$.

2.5 VISIBILITY FOR NON-PARAXIAL OBSERVATIONS OF PARTICLES WITH SIZES MUCH GREATER THAN A WAVELENGTH

In evaluating the visibility for spheres, it was tacitly assumed that the observation of the scattered light would depend on the total flux incident on the particle. This should be a reasonable assumption as long as the observations are not biased by reflection and refraction effects (i.e., when the particle sizes are less than 4 to 5 λ_o) and the observations are made paraxially. However, when sizes are greater than 4 to 5 λ_o, then effects related to Snell's law (i.e., reflection and refraction)

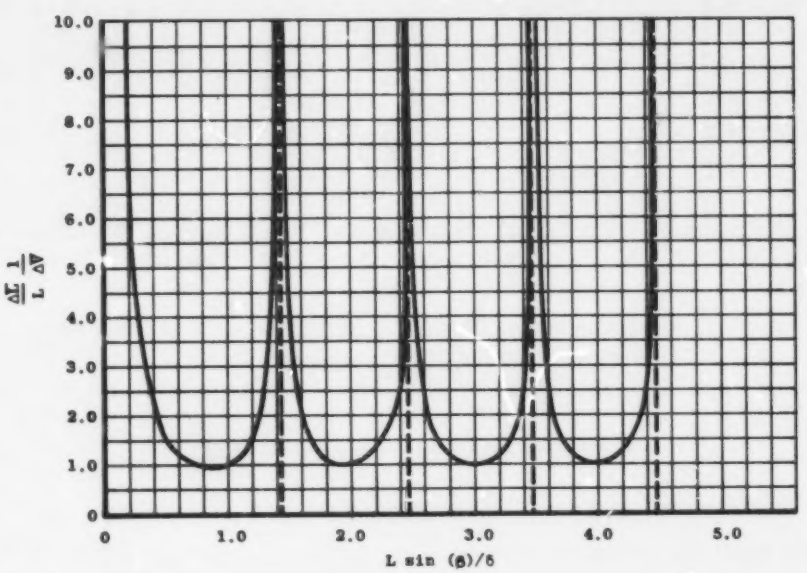

Figure 10. Uncertainty curve for a long narrow cylinder with size determined by a visibility measurement.

can play a significant role in determining observation limits imposed by the scattered light viewing system. It has been shown (Ref. 11) that for large particles observed non-paraxially, evaluation of Eq. (4) requires that the limits of integration be changed to include only a portion, rather than all, of the particle's cross-sectional area. Figure 11 plots an example of the visibility calculated for a particle, large compared to λ_o, for an observation angle 10° off axis. For comparison, the paraxial visibility is also plotted as a dashed line. The figure shows that for such large particles, observed non-paraxially, the visibility can give only ambiguous values of particle size. This complication can be avoided by making all observations paraxially.

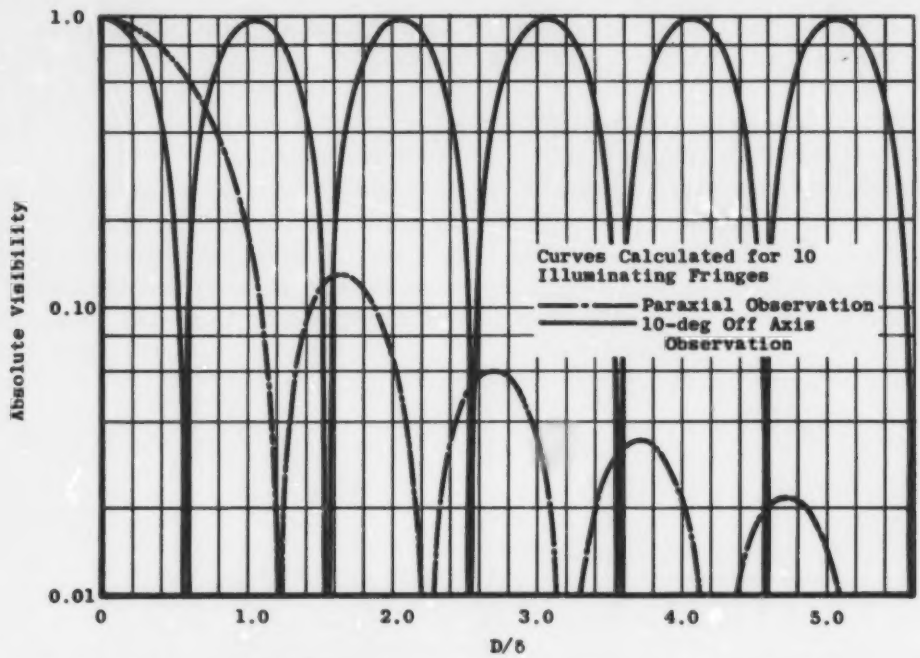

Figure 11. Visibility for non-paraxial observation of a large particle compared to illuminating wavelength λ_o.

3.0 EXPERIMENTAL OBSERVATIONS

In this section the results of an experimental program to determine the feasibility of dynamic particle size analysis from the interferometric visibility techniques are described and discussed. The experiments were conducted on particles in the size range 1.0 to 120 μm. It

was not surprising to find that the large particles required an entirely different set of experimental observations and methods than did the small (less than 4 to 5 λ_o in diameter) particles. Thus, a natural point of division in discussing the experiments is in the large and small particle observations.

3.1 EXPERIMENTAL EVALUATION

A schematic of the optical arrangement for the experiments is shown in Fig. 12. Light from a 15-mw He-Ne laser has its polarization vector rotated until it is perpendicular to the plane of the beams defining the probe volume. Collimating lenses then cross the beams and focus them simultaneously. Two types of beam splitters were used in these experiments. The first type is a set of properly coated glass blocks, shown in the photograph in Fig. 13, which produce two beams that (1) traverse equal path lengths, (2) are of equal intensity, and (3) have centerlines parallel within a tolerance of a few arc-seconds (Ref. 15). The second type of beam splitter is a two-dimensional, ultrasonic modulator operated in a traveling wave Bragg mode (Refs. 5 and 16). This device can produce four equally intense frequency shifted beams (the frequency shifts are identical to the modulator frequency). If both acoustic modulators are referenced to a common oscillator, stationary interference fringes can be generated in the probe volume by two of the beams. When the modulators are referenced to two different oscillators, the interference fringes move at a rate which is the difference frequency between the two oscillators. Such a device gives the capability of positioning stationary particles in the probe volume and moving the fringes past the particle. This is most desirable when the particles are small ($<5\lambda_o$) and not easily located. A schematic of a two-dimensional Bragg cell (TDBC) particle-observation system is shown in Fig. 14.

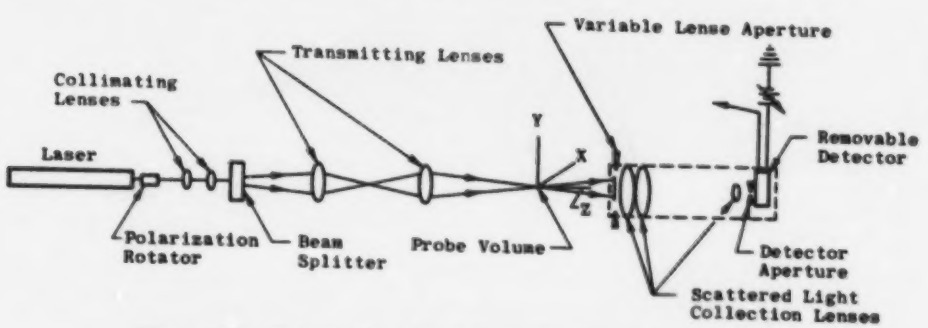

Figure 12. Schematic of the optical arrangement for the experimental observations.

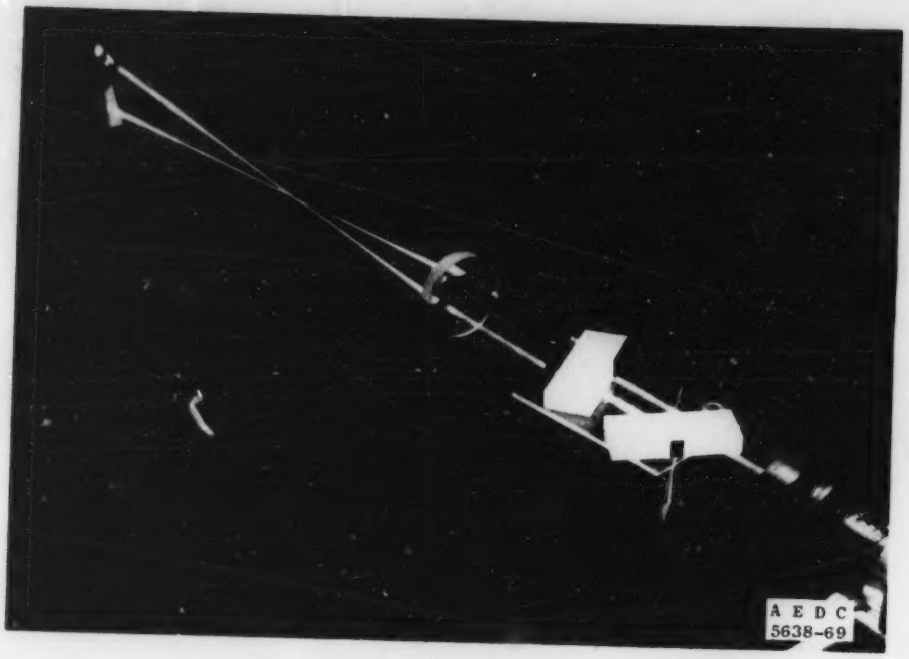

Figure 13. Photograph of path compensating beam splitting blocks.

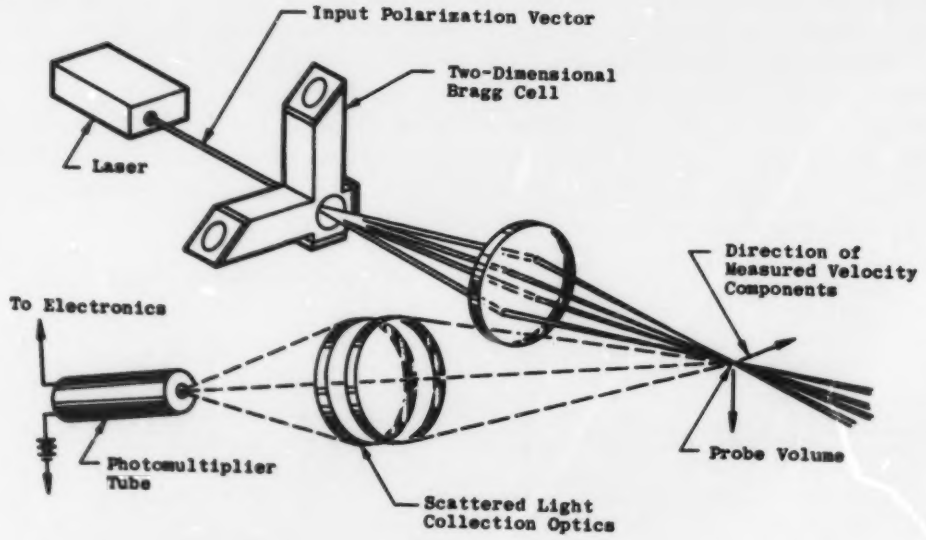

Figure 14. Schematic of the two-dimensional Bragg cell arrangement.

After the beams are split, a set of lenses positions the probe volume to the desired observation region. The scattered light collection optics are designed and mounted such that almost any desired set of observation angles can be obtained while observing the same portion of the probe volume. When the collection aperture is fully open, an f/5 solid collection angle is subtended. A variable aperture is also placed in front of the detector to control stray light and to determine the size of the observable probe volume. The beam stops and detector are removable in order to allow visual observation of the interference fringes by paraxial projection through the scattered light collection telescope. Figure 15 shows a photograph of the overall optical system.

The large spherical particles used in these experiments were glass and aluminum spheres. Tungsten wires of varying lengths having a diameter of 11.6 μm were also used in the experiments. To control the position of the particle as it traversed the probe volume, a traverse system was used which had a positional accuracy of ± 1.0 μm along the z axis and ± 5.0 μm along the y axis. The spheres were mounted by electrostatic

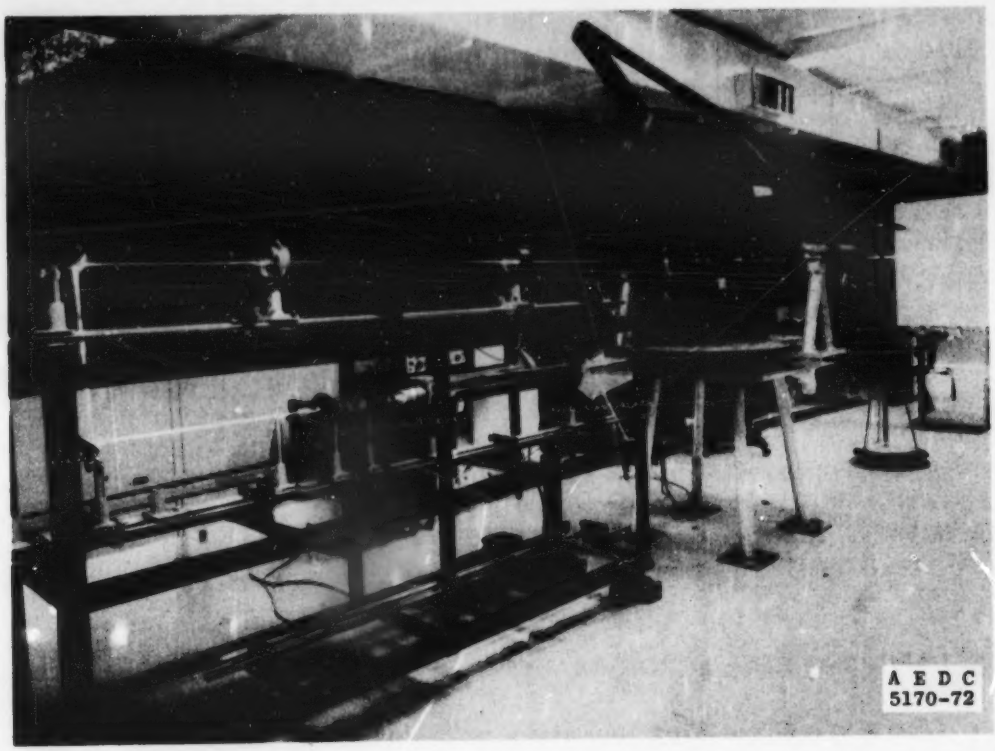

Figure 15. Photograph of the overall optical system.

attraction (van der Waals forces) on coated optical flats. The flats were then mounted vertically with micropositioners on the traverse system. The particles were visually positioned as desired in the probe volume by observing the projected image either through the scattered light collection telescope or through a microscope with a calibrated reticle. Thus, fringe spacing and particle diameters could be measured directly for comparison against the visibility measurements. The y axis portion of the traverse could be released from the mechanical crank drive and pushed by hand smoothly on ball bearing rollers. Hence, particle trajectory relative to the geometric center could be precisely controlled. Presumably, the velocity of the particle could be assumed constant during the short time interval the particle was in the probe volume. The 11.6-μm wire was mounted in a similar fashion, except no glass plate was used (the wire was stretched across an aperture). A micropositioner could vary the angular orientation of the wire (β) about the z axis with an angular precision of ±30.0 arc-seconds. The wire served two purposes in these experiments. First, for a large fringe spacing and $\beta = 0$, the wire served as an integrating probe (in the sense that the wire averaged the entire light distribution along the major axis of the interference fringe) through which the illuminating intensity distribution could be studied. Secondly, by suitably imaging the fringes at the detector, various orientations of the wire provided straightforward experimental verification of Eq. (9). The particle-holding jig and traverse system are shown in the photograph in Fig. 16.

Scattered light signals detected with a photomultiplier tube were filtered and amplified with a variable bandpass differential amplifier and were recorded on a storage oscilloscope. From the oscilloscope, the signals were photographed for measurement analysis using Eq. (11).

For stationary particles with interference fringes moving past them, a continuous wave signal of constant amplitude was generated. Thus, the a-c signal values could be measured directly with an RMS voltmeter while the d-c level of the signal could be measured either with an electrometer or with the oscilloscope set for a zero width frequency bandpass. With this arrangement an average over many cycles of information could be obtained for one particle position in a short time interval.

3.2 LARGE PARTICLE ERROR ANALYSIS

The accuracy of this technique in determining particle sizes depends in large measure on how well the interference fringe spacing is

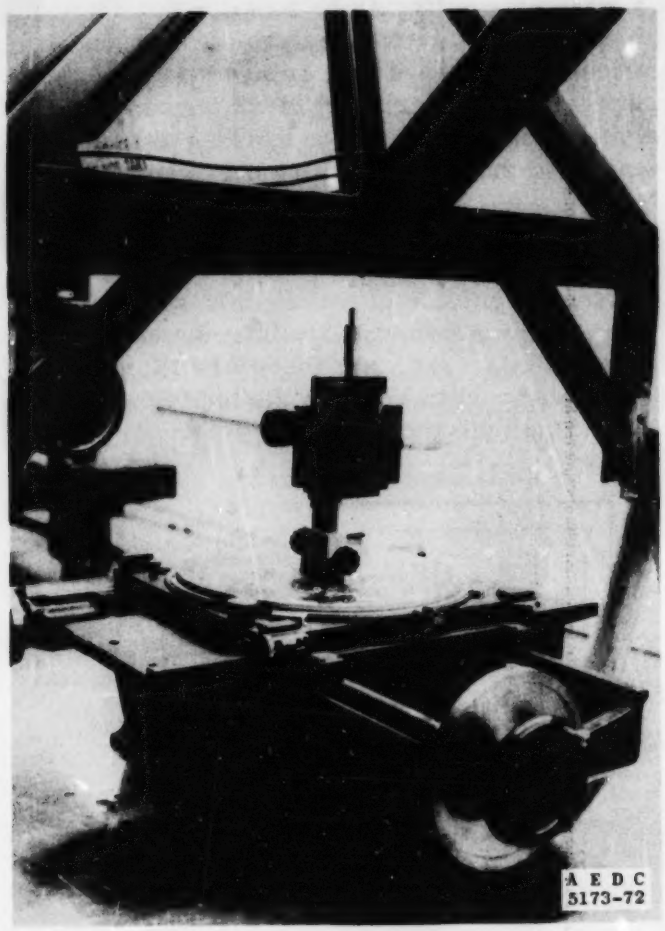

Figure 16. Photograph of the particle holder and traverse system.

known. For these experiments, the fringe spacing was measured by two independent techniques. In the first method, the fringe spacing was determined by measurements of an image projected through a microscope which also projected the image of a calibrated reticle. Comparison of the reticle period with the interference fringe period provided a measure of the fringe spacing. In the second technique, use is made of the fact that the fringe spacing, δ, for $\alpha << 1$, can be written as

$$\delta \simeq \lambda_o/a \tag{26}$$

α in these experiments was typically between 0.5 to 3.0° and could be measured with an uncertainty of about ±2 percent. λ_o is known to at least six significant figures. Thus, fringe spacing could be measured by this technique with an uncertainty of ±2 percent. Generally, the two separate determinations of the fringe spacing agreed within ±3 percent, which was considered sufficient for these experiments.

The largest source of error in the experiments was in the analysis of the photographs. Since the oscilloscope traces were measurably wide relative to the magnitude of the signal, some uncertainty in the values of the signal was automatically introduced. The amount of data to be reduced was voluminous, and therefore the data reduction system shown in Fig. 17 was used to analyze the photographs and to perform various manipulations with the recorded data. X-Y positions of points

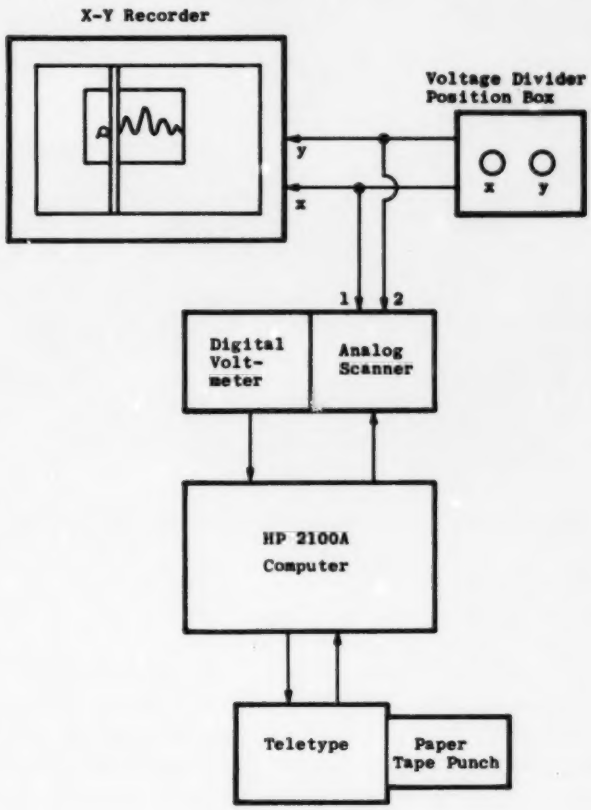

Figure 17. Schematic of the data reduction system.

on the photographs were proportional to a particular voltage as determined by the X-Y recorder and a voltage divider box. The value of the voltage for a particular measurement point was read by a digital voltmeter and the value stored in the computer memory for recording on punched paper tape. Additional uncertainty was, therefore, introduced into the measurement by any uncertainty in the voltage measurement. Furthermore, error enters into the measurement due to slight distortions introduced into the image in the photographic process. In order to determine the magnitude of the uncertainty in these measurements, the data reduction system was used to scan a photograph of the grid face present on the oscilloscope. The result showed that the measured visibility was uncertain by ±3 percent.

3.3 EXPERIMENTAL RESULTS OF LARGE PARTICLE OBSERVATIONS

The geometric center of the probe volume and the relative illuminating intensity distribution are fundamental parameters which must be known if accurate particle sizes are to be obtained from visibility measurements. Knowledge of the spatial position of the geometric center is required if accurate fringe spacing measurements are to be made from the measurement of angles technique. Equation (3) and subsequent analysis show that contrast variations in the illuminating intensity distribution can be expected as the distance from the geometric center increases. Furthermore, Eq. (3) is for an ideal focusing condition; thus, some deviation from the ideal focus case might be expected for the lenses used in the experiment. The mounted wire discussed previously was used to probe the intensity distribution for a fringe set with a spatial period much greater that the wire diameter. The observed signal scattered from the probe represented an average intensity along the major axis of the fringe. Since the intensity distribution is Gaussian along the major fringe axis, the averaged intensity distribution was representative of the y-z plane intensity distribution. Figure 18 contains a theoretical plot ($x = 0$, $\delta \simeq \lambda/\alpha$) of the y-z plane intensity distribution for different values of z where z is written in terms of a dimensionless depth of field parameter (Ref. 8) m:

$$m = z \sin(\alpha/2)/b_o \qquad (27)$$

(Thus m = 1.0 where the edge of the defined probe volume crosses the x axis.) The corresponding experimental scans with the small wire are also shown for qualitative comparison. To keep the diagram from being too cluttered, theoretical plots are shown for six cycles of information

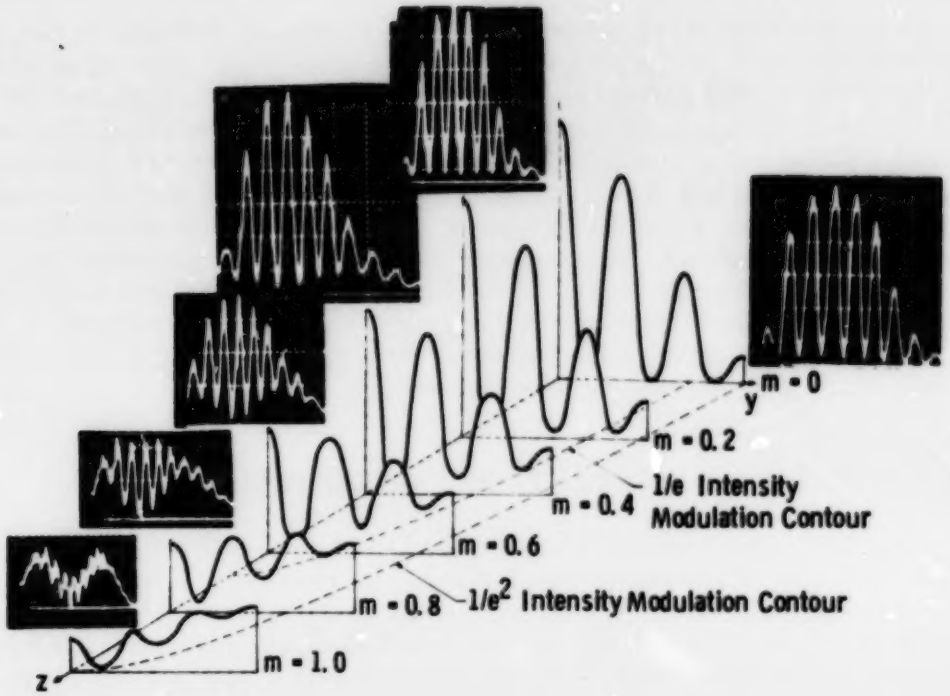

Figure 18. Experimental and theoretical illuminating intensity distribution in the probe volume.

between the e^{-2} relative intensity points along the y axis passing through the geometric center. The experimental scans are for approximately ten cycles of information; quantitative comparison in this case is circuitous. However, when a comparison is made with identical numbers of interference fringes in both theory and experiment, calculated and measured visibility for random checks of different fringe points agree within a few percent. The observed fringe visibility at m = 0 is about 0.95. This is attributable to an intensity mismatch of the illuminating beams. This mismatch was not attributable to the beam splitter but rather to the complex phase variations introduced into the beams by the transmitting lenses. This effect is also reflected in the slight skewness of the Gaussian envelopes and in the apparent phase changes of the fringe position as m varies. These effects could be controlled through the use of diffraction limited lenses or carefully controlling the orientation of lenses of inferior quality relative to the incident beams.

An experiment was performed to determine the validity of Eq. (9). A slit aperture placed in front of the signal detector was oriented normal to the projected image of the interference fringes. The fringe spacing was chosen to be 109 μm. The width of the slit was set to 500 μm. Hence, as the wire was rotated through the angle β, a very narrow cylinder of length L and orientation β, was observed. L was related to the magnified width of the slit w′ and orientation angle through the relationship

$$L = w'/\cos(\beta) \tag{28}$$

Substitution of Eq. (28) into Eq. (9) shows that the visibility is then given by (paraxial or small angle approximation)

$$V = \frac{\sin[\pi w' \tan(\beta)/\delta]\ \sin[\pi D \cos(\beta)/\delta]}{[\pi w' \tan(\beta)/\delta][\pi D \cos(\beta)/\delta]} \tag{29}$$

Figure 19 contains a graph of Eq. (29) as a solid line between one and the first zero in V for the parametric values of w', D, δ, and β.

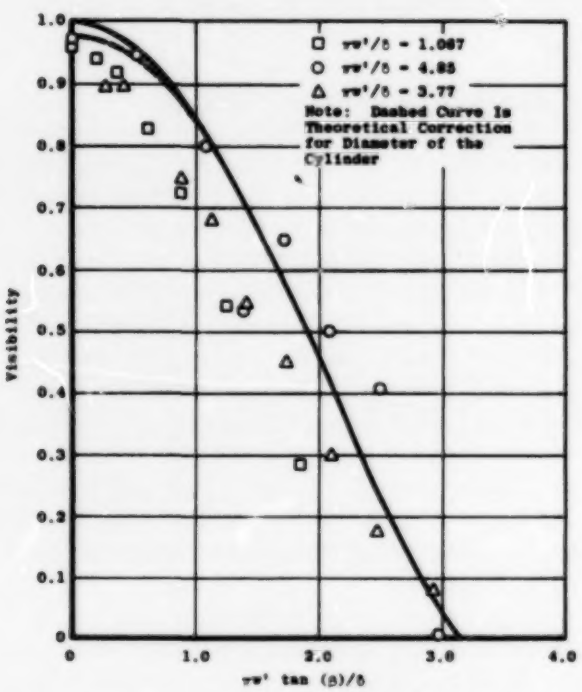

Figure 19. Experimental and theoretical comparison for a long narrow cylinder at different orientation angles

Experimental points are indicated with circles, squares, and triangles for three values of $\pi w'/f$. As can be seen in Fig. 19, reasonable agreement exists between theory and experiment. The primary cause of the deviation from theory are uncontrollable variables in this particular observation technique. The measurements were carried beyond the first zero in V. However, systematic error was found to be comparable to the measured visibility. Therefore, these results are not included for any valid comparison with theory.

Observations of large, single spherical particles have also been made. For particle sizes greater than 90 μm, spheres of aluminum and glass were examined. When the diameter was less than 90 μm, only glass spheres were available. Observations for different solid collection angles were made to determine any visibility dependence in terms of observation angle resolution. Front scatter measurements were made for different angles of observation with respect to the bisector between the beams in order to determine visibility dependence on these parameters. Signals attributable to different trajectories of the particle traveling in the y-z plane and normal to the z axis were also observed in order to determine practical depths of field for those observations.

Figures 20 through 22 summarize the results. The solid curve in Fig. 20 indicates the theoretical visibility for a particle at the geometric center of the probe volume. Data points for both glass and aluminum spheres are plotted as circles and squares, respectively. The data show that reasonable agreement with theory is obtained for both types of particles when D/δ is less than or approximately equal to unity. Large deviations are observed when the particle diameter is comparable to the diameter of the probe volume, even when D/δ is about the right magnitude (note the data points inside the dashed square). This should be expected on the basis of the assumptions expressed by Eq. (5). Some deviation can also be attributed to reflection and refraction biasing the signal and contributing significantly to the signal when the particle is not fully illuminated. Some systematic error is also apparent for $D \lesssim 0.5\ \delta$ and is believed to be attributable to calibration errors in measuring particle size for comparison with the visibility measurements.

Figure 21 shows how the average visibility varies as a function of the depth of field. It shows that there is little variation in visibility when the particle size is of the order of a fringe spacing and the trajectory is within $m = \pm 0.2$ (Eq. (27). This is consistent with numerical

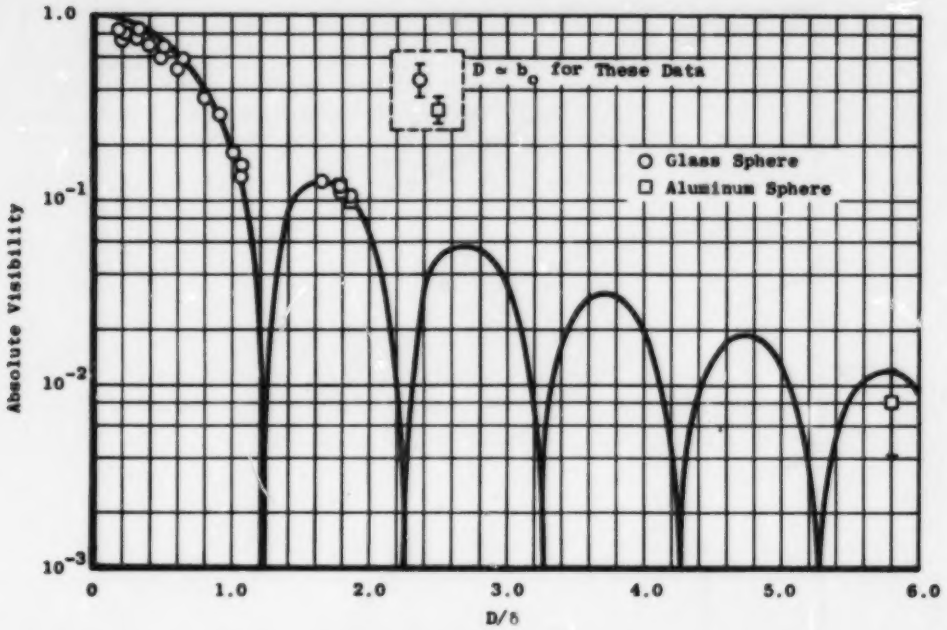

Figure 20. Comparison of theoretical and experimental paraxial visibility for a spherical particle.

evaluations of Eq. (4). Also plotted in Fig. 21 is the average visibility for a point particle passing through ten interference fringes. It is seen that the m = ±0.2 criterion defines a relatively error-free region in both cases (for experimentally large particles and for a theoretical point particle) wherein size can be determined from Eq. (8) or Eq. (9).

Figure 22 indicates the results of making observations for different solid collection angles to determine any visibility dependence. The plots show the visibility independent of solid collection angle over more than three decades of variation.

To test the validity of Eq. (16) which predicts the variation in the visibility as a function of number of illuminated particles, the following experiments were performed. The interference fringes were adjusted for 120-μm separation distance. Glass spheres 10 to 15 μm in diameter were randomly spread over the glass plate formerly used to hold the single large particles. The glass plate was then mounted vertically on the holding jig such that it could be moved through any probe volume position. The TDBC was first arranged to provide moving interference fringes. The glass plate was randomly searched for regions where the scattered light intensity was high or relatively low, which indicated high or low concentrations of particles.

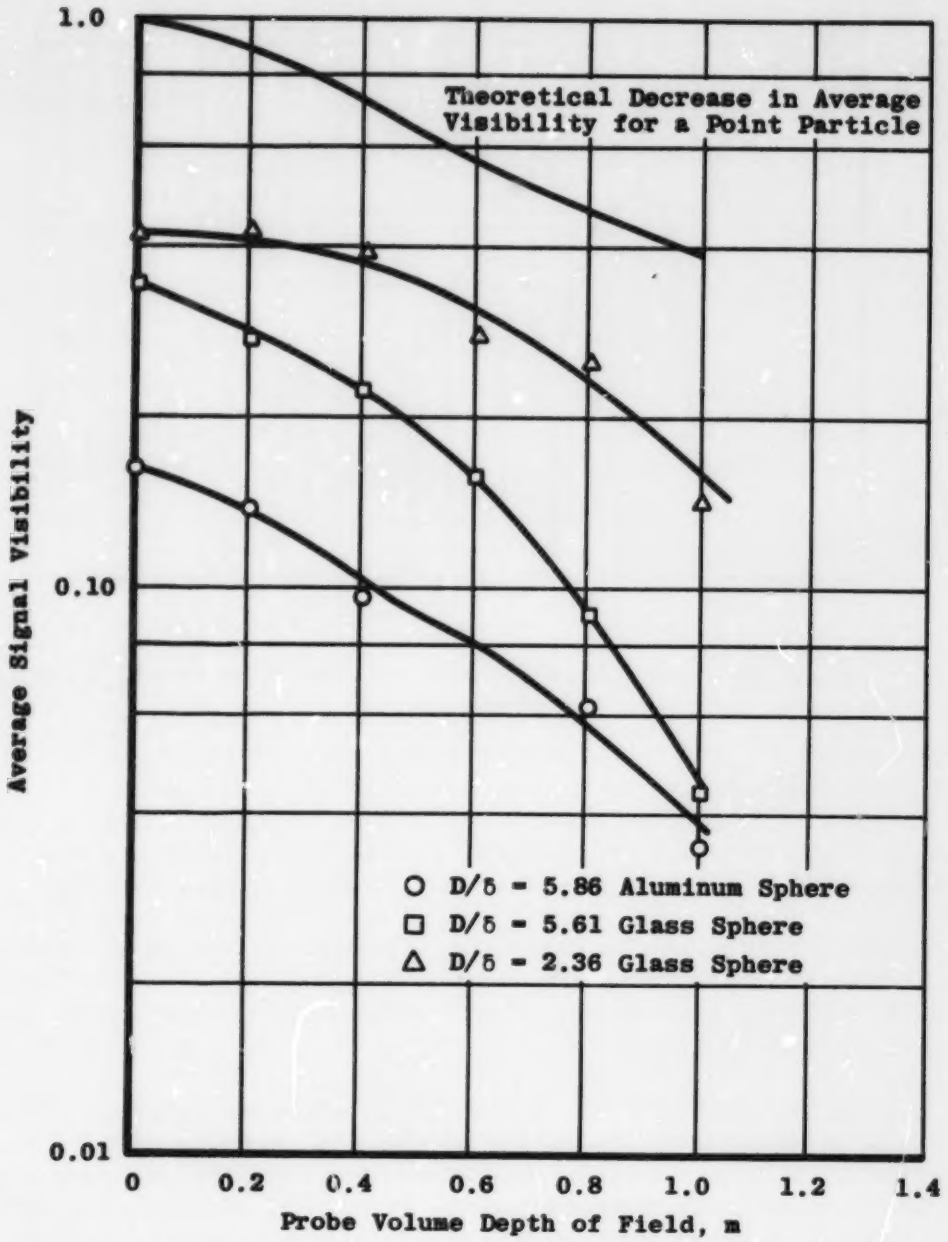

Figure 21. Average signal visibility as a function of particle trajectory for different D/δ.

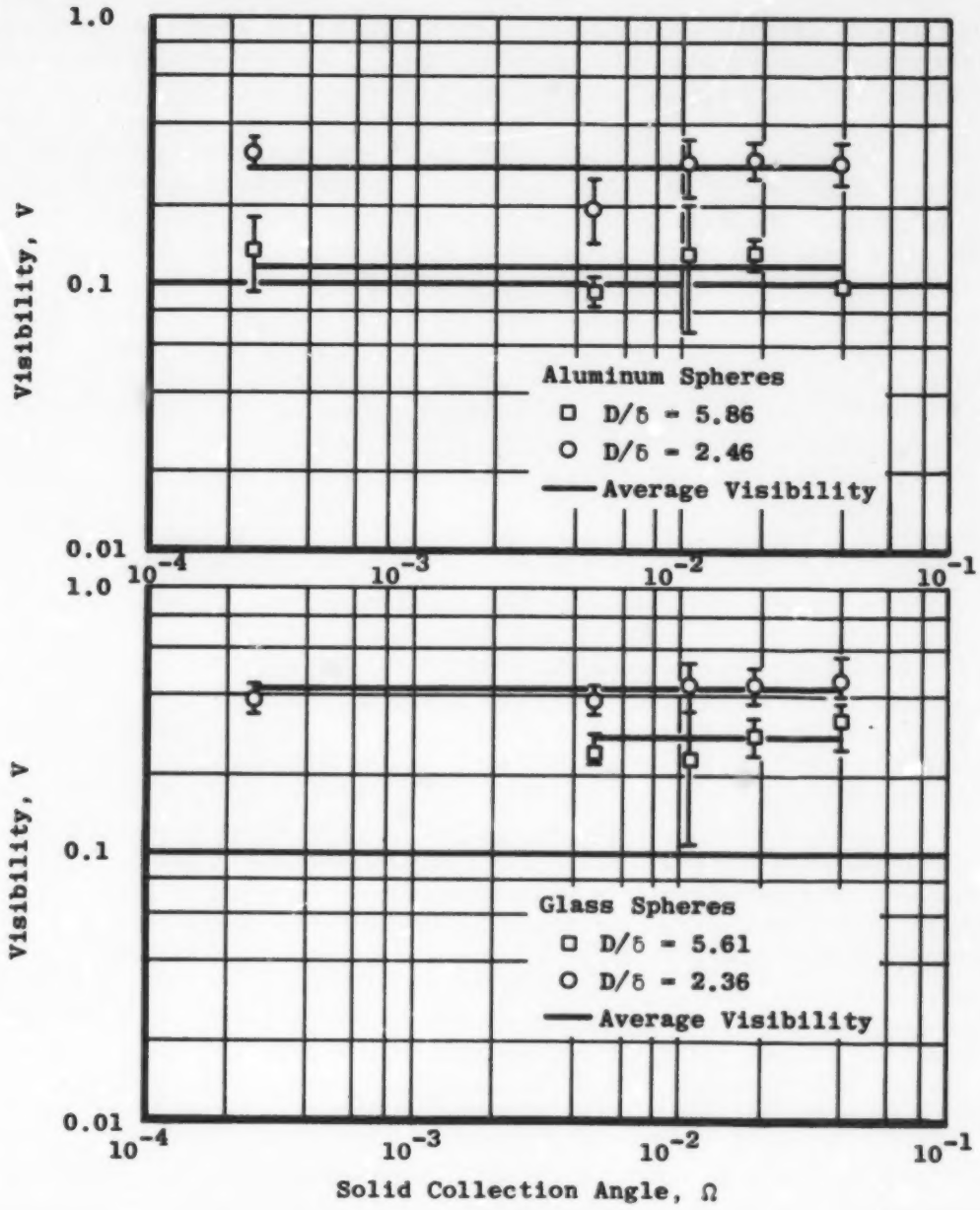

Figure 22. Variation of visibility for different D/δ and solid collection angle.

Once a particular plate position was selected, an image videcon tube was mounted in the position formerly held by the PM tube in the light collection system. The scattered light collection system was used to image the particles illuminated on the glass plate onto the image videcon tube which in turn displayed the image on a TV monitor. Thus, the number of particles being illuminated and their relative positions could be determined either by visually counting the particle images or by using an electronic computer system which was available. The computer and associated electronics could be set to automatically count the number of images having an intensity level greater than a preset value. The number of images as determined by the computer was then displayed on the TV monitor along with the images observed by the videcon tube. The computer system also caused the TV display to indicate which images had been counted in order to allow the preset image intensity to be consistent with the experimental requirements (in this case, those images which could be observed to exist within the probe volume cross section of illumination).

The TV monitor image was photographed as was the computer-measured image. The image videcon tube was then removed and a PM tube put in its place. Only the scattered light was allowed to enter the PM tube. The particle positions and optical system were otherwise undisturbed from that observed with the image videcon tube. The scattered light signal from the interference fringes moving past the particle array observed with the image videcon was displayed on an oscilloscope and photographed. Ten different particle arrays were observed in this fashion. Figure 23 presents the photographs obtained from these observations. Each row represents a single set of observations. The photographs are (reading left to right) the TV monitor image of the array, the computer-counted image of the array, and the scattered light signal. To the left and right of the photographs is the computer-counted number of particles and the number determined from the visibility measurement. Agreement is seen to exist between the values determined from the two separate measurements in only a few cases. Variations between the two are to be expected on the basis of size variations in the number of particles observed at any one time.

In order to examine the changes in the visibility as the number of particles in the probe volume kinematically changes, the following experiments were performed. Diametrical scans of about 6 cm in length were made across the face of the glass plate containing the glass particles. The scans were always across the same diameter and were made for stationary interference fringes of the same period as in the previous

multiple particle experiments. Thus, as the plate, which contained varying numbers of particles across the scanned diameter, traveled through the cross section of the probe volume, the kinematic evolution of the signal attributable to varying numbers of particles could be

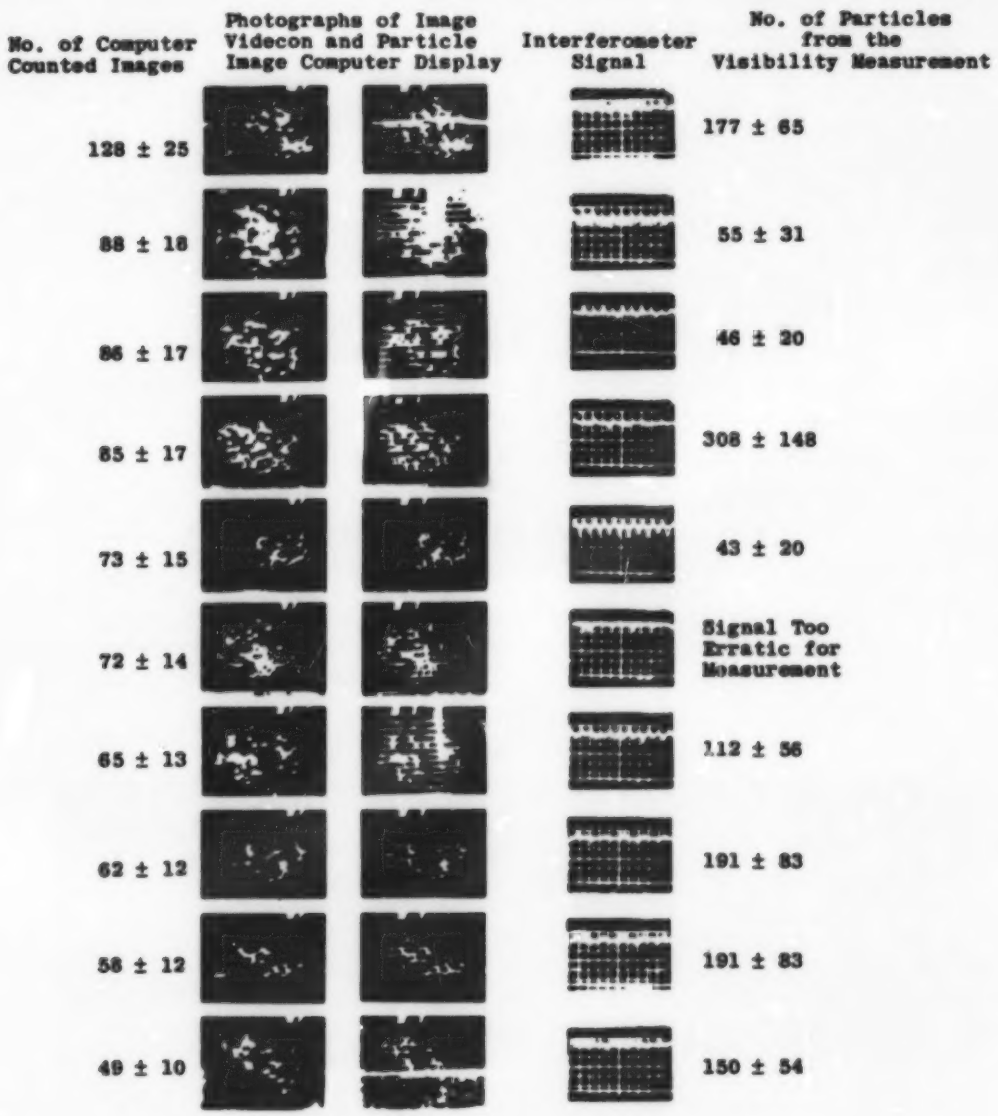

Figure 23. Comparison of number density measurements by image computer with those made by an interferometer.

observed. Since the signal lasted about twice as long as the sweep time of the oscilloscope, two oscilloscopes triggered in sequence were used to record the signal. The respective signals were then photographed and then matched in sequence to provide a complete time history of the particle scan. To determine the number of particles in the probe volume, for a comparison with instantaneous visibility measurements, the PM tube was replaced with the image videcon tube and the entire particle distribution across the plate diameter photographed and number of images sampled and counted by the computer. Figure 24 is an example of the observed scattered light signal as determined by the oscilloscope recordings. The scattered light signal was observed for different light collection solid angles and for different angles of observation in the y-z plane. The results revealed the following:

1. The visibility for N particles is not a function of solid collection angle.
2. The visibility for N particles is a function of observation angle when the particles are large; the dependence seems to be a reflection mechanism that is similar to that observed for single large particles.
3. Number density can be determined for size distributions when the distribution is sufficiently narrow (this sufficiency condition has not been determined analytically).
4. There appear to be phase reversals in the signal for certain spatial combinations and numbers of particles. The conditions for the reversal to occur have not been determined.

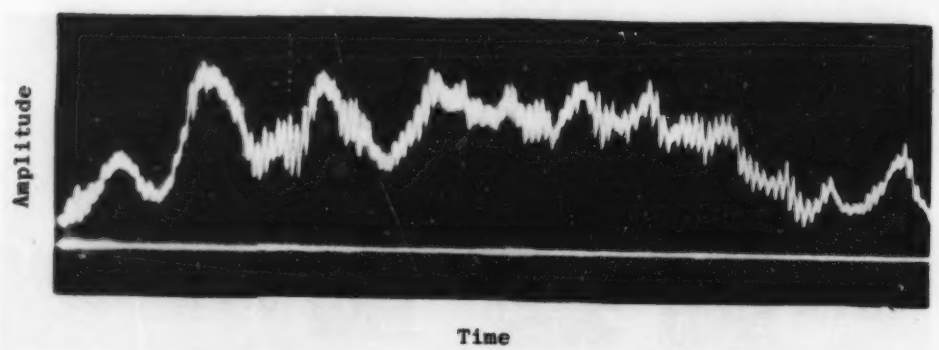

Figure 24. Photograph of interferometer signal versus time as the number of particles passing through the probe volume changes.

The results from the experiments show (at least for particle sizes greater than about 10 μm) that with additional development the number density can be determined from visibility measurements.

3.4 EXPERIMENTAL RESULTS OF SMALL PARTICLE OBSERVATIONS

Experiments involving small particles (diameters less than about 2 μm for visible light) required several different approaches than those involved in the large particle observations. The transition from self-aligning to non-self-aligning optical systems must be made in order to obtain small fringe periods. The result is an optical system which is subject to alignment errors and is vibration sensitive. When non-self-aligning systems are used, the interference fringe period can no longer be measured with a microscope projection system. The fringe period must then be determined from a measurement of the included angle between the beams. The most difficult practical limitations to such experiments, however, were in (1) the generation of consistent particle sizes, (2) the realization of a well controlled trajectory, and (3) the use of some other method to measure the particle size for comparison with the visibility measurement. Therefore, by comparison with the large particle measurements, those of the small particles were crude and the associated errors disproportionately large.

The non-self-aligning optical arrangement shown in Fig. 25 was used to examine particle sizes less than 2 μm. Lenses L_1 and L_2 focus the two beams and mirrors M_1 and M_3 simultaneously cross the beams. The probe volume location is determined by the beam splitter and mirrors M_1, M_2, and M_3. The scattered light is detected paraxially by lens L_3 and the photometer system. Since the system is non-self-aligning, the quality of the interference fringes depended on manual adjustments of M_1 and M_2. Such adjustments did not present any undue difficulty.

Two approaches were taken to resolve the particle control problem. Polystyrene latex spheres of less than 2.0-μm diameter, manufactured by the Dow Chemical Corporation, were used. These particles are sized with an electron microscope and were specified to have a standard deviation of 0.0027 μm and were specified spherical. They were measured by the interferometer in a water solution. The water base for the particles

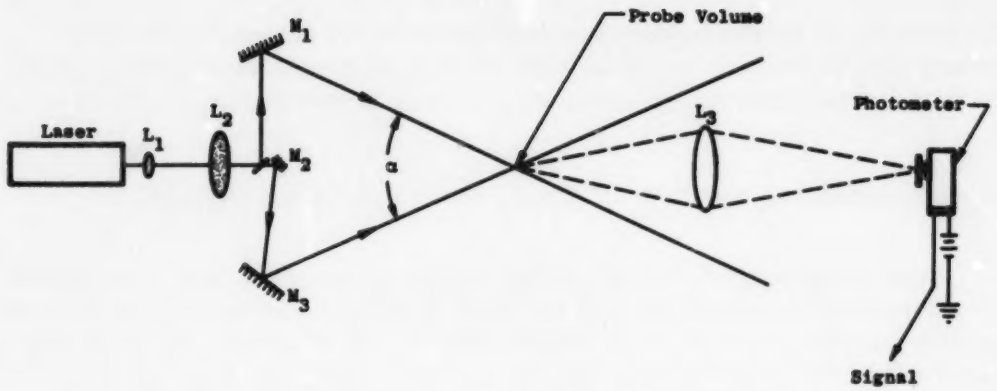

Figure 25. Experimental arrangement for small particle observation.

was initially filtered to remove all extraneous particles with sizes greater than the 0.2 μm. The second approach involved statistical inference and has much less control than the latex sphere experiments. In this approach, particles present in laboratory air were examined. A large circular window was cleaned and placed on edge in the proximity of the probe volume for seven days. At the end of this period the window was examined with a 400X microscope. The overwhelming number of observable dust particles collected on the window were either spheres or "fat" cylinders of aspect ratio (length/diameter) 2:1 and approximately 2.5 μm in diameter. Particles larger than 2.5 μm were generally found to be highly irregular in shape, although shapes tended to cylindrical symmetry with aspect ratios varying between 1.5 to 4. Large numbers of particles present in the laboratory air were examined with the interferometer and the visibility and signal magnitude recorded. These measurements were then compared with the microscope observations.

Two different fringe period settings were used in these experiments. The fringe periods for the particle measurements in air were 3.5 μm and 1.22 μm. Probe volumes in air were computed to be 2.75×10^{-5} cc and 9.63×10^{-6} cc, respectively. In water, these values are reduced by a factor of 2.35 due to the index of refraction. Approximately 100 interference fringes for the large probe volume and 200 for the small one were observed.

Measurements of the latex spheres in the water suspension were difficult because of index of refraction variations and low frequency

vibrations. Visibility measurements gave an indication of particle diameters between 0.50 μm and 0.65 μm. However, the data were of insufficient quality to be valid.

The number of particle signals from laboratory air per unit time as a function of signal amplitude was determined. Under the assumption that the signal amplitude is proportional to the cross-sectional area of the particles, an estimate of the relative particle size distribution can be obtained. A plot of the normalized number density versus relative size (relative to the smallest size observed) based on the above assumption is given in Fig. 26. For example, from Fig. 26, 1.0 particle per second was observed with a diameter in the range from 1.00 to 1.22. For a given amplitude range, approximately ten signals were observed and signal visibility measured.

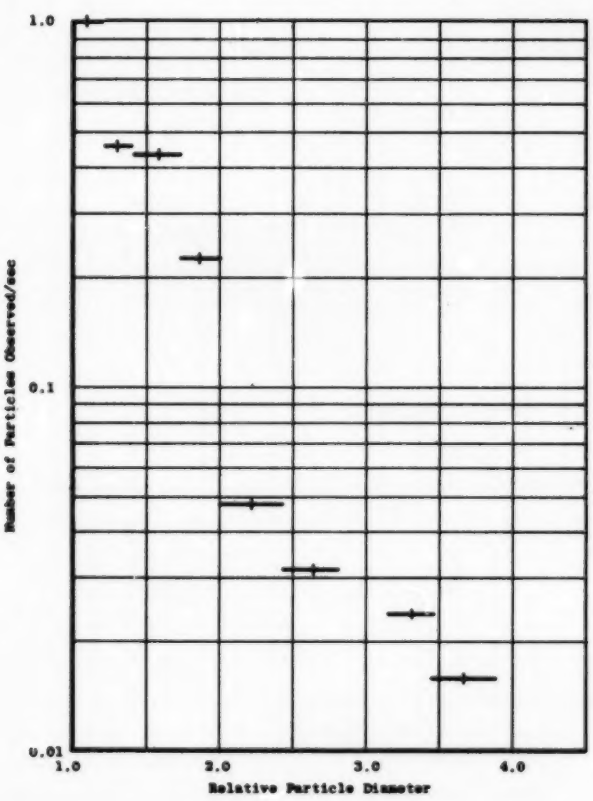

Figure 26. Relative particle size distribution of laboratory particles.

Fringe spacing δ was 3.4 μm. Histograms of number versus visibility for these observations are shown in Fig. 27. Without knowing particle shape, little quantitative information about particle size can be verified from the histograms. For the larger particles (as determined from the signal amplitudes), the large variations in the visibility suggest irregularly shaped particles. If the smallest particles are spheres, the size range described (visibility between 0.2 and 0.5) lies between 2.4 μm and 3.4 μm which is in good agreement with the microscope observations of the window-collected dust particles.

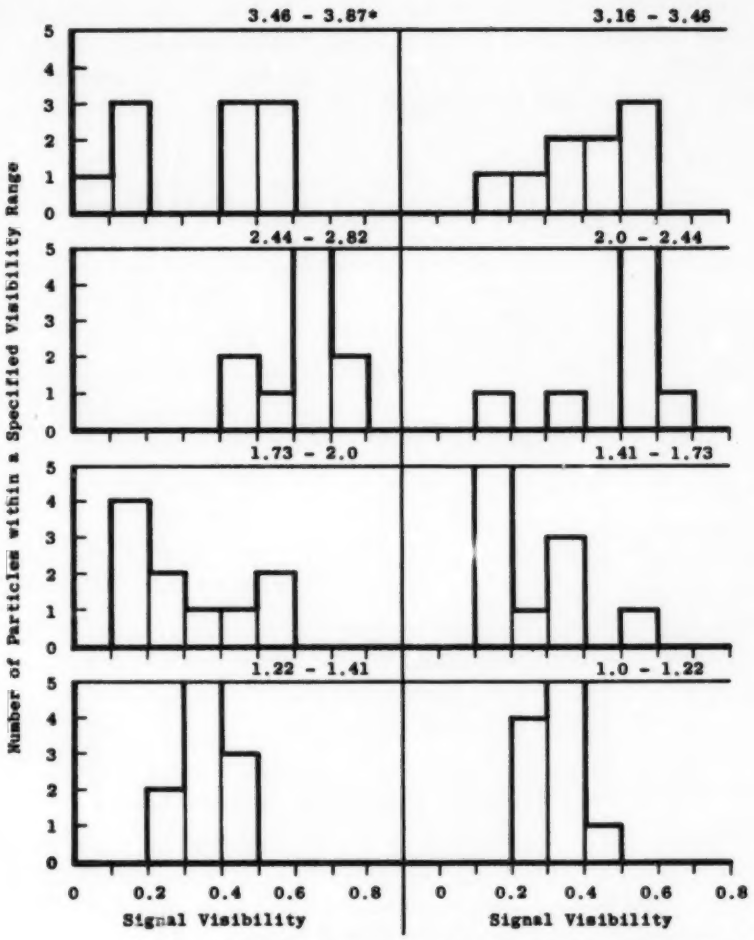

Figure 27. Particle visibility histogram for laboratory air particles.

4.0 ELECTRONIC INSTRUMENTATION

4.1 GENERAL

A primary result of this research is the graphic demonstration of the need for an electronic device which can automatically determine the visibility from the input signal. Without the development of such an instrument, the utility of this method of particle size analysis is greatly limited. Therefore, preliminary work was initiated to determine design concepts which would be most appropriate for the scattered light signals. Two design approaches have been taken. The first separately measures the peak values reached by the a-c component and the pedestal; the ratio of these two peak values is then taken to form the visibility. The second approach continuously measures both the a-c and pedestal magnitudes and ratios these values, providing a continuous visibility measurement over the signal waveform.

4.2 VISIBILITY FROM PEAK VALUES

Peak values separately reached by the a-c and pedestal components may be used to measure the visibility. This assumes optical aperturing is used so that the light collection optics see only particles whose trajectories lie close to the x-y (z = 0) plane which passes through the center of the probe volume. In this region, visibility remains fairly constant and is a function of particle size alone. The ac and pedestal rise and peak at the same time, and signal waveforms look like those shown in Fig. 3. In this method, filters are used to separate the ac from the pedestal as shown in Fig. 28. Peak detectors are used to measure the peak values reached. The a-c peak is then divided by the pedestal peak

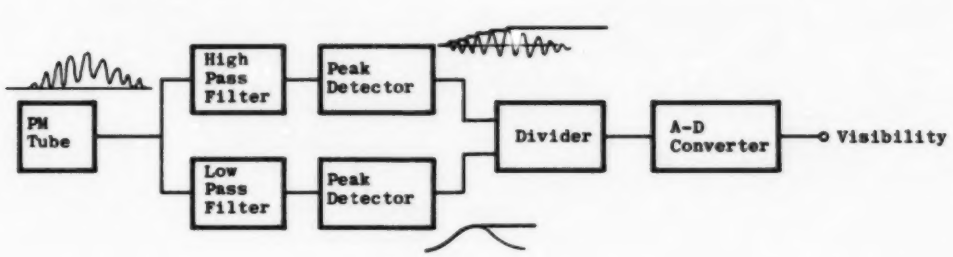

Figure 28. Electronics for visibility measurement from peak values.

in an analog divider to form the visibility. The visibility is converted to digital form for storage until it is ready for output. The method of using peak values has some inherent disadvantages as follows:

1. Optical aperturing must be used but is difficult to achieve.
2. There is no way to know if a noise spike raises a peak value, giving an erroneous visibility.
3. Frequency response of peak detectors has been found to be limited to about 5 MHz. If higher frequencies are to be used, frequency down-conversion must be used prior to the detector, which introduces additional non-linearities and extraneous signals to be dealt with.

4.3 CONTINUOUS MEASUREMENT OF SIGNAL VISIBILITY

Because of the disadvantages encountered in the first method described above, a second method is now being developed. This approach is designed to take advantage of the fact that the visibility remains fairly constant in the region of the x-y plane, where it is desired to measure the visibility. In this method, shown in Fig. 29, the a-c and pedestal components are again separated by filters. An envelope detector is used in the a-c channel to extract the envelope of the ac, i.e., a signal proportional everywhere to the magnitude of the ac. The a-c magnitude is divided by the pedestal in an analog divider, and the visibility is continuously output from the divider throughout the particle's

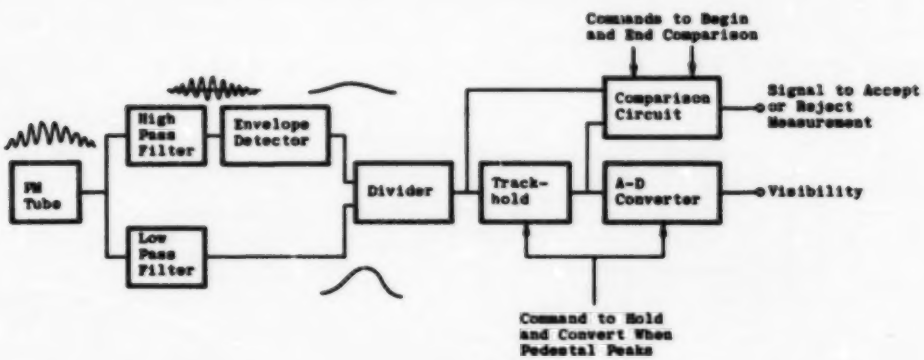

Figure 29. Electronics for continuous measurement of visibility.

traversal of the probe volume. At some point on the trajectory (e.g., when the pedestal reaches a peak) the visibility is recorded by a track/hold module (sample/hold) and converted to digital form. This recorded value is then compared with the visibility subsequently output from the divider as the particle proceeds along its trajectory. Comparison is continued for a period of time, e.g., until the pedestal has fallen to some preselected value.

If the visibility does not vary more than some preselected amount while the comparison is being made, the particle probably passed sufficiently close to the x-y plane for the visibility measured to be valid. If the visibility varies more than the amount selected, either noise perturbed the signal or the particle passed too far from center, and the measured values are rejected. Aperturing is thus achieved electronically and noise-perturbed signals are rejected. Further, the envelope detector has a higher frequency response than the peak detector and frequency down-conversion is not necessary.

The electronic instrument for visibility measurement is still under development, and extensive testing will be required to confirm the best method to be used.

5.0 SUMMARY AND CONCLUSIONS

The results of the research described in this report are best summarized in terms of parameters which were examined during the course of the analytical and experimental work.

5.1 PASSAGE ANGLES OF THE PARTICLE THROUGH THE INTERFERENCE FRINGES

In order to use the expressions for the visibility developed in this report, it is necessary that the visibility be measured in a specified region sufficiently near the plane $z = 0$ (x-y plane); this plane passes through the center of the probe volume. Optical aperturing may be used to detect only light that originates near the x-y plane, or alternatively, as described in Section 4.3, electronics may be used to select only signals originating in this region. There is no other limitation on the particle's trajectory except that for systems without moving fringes the particle must move across the fringes in order for the signal to be adequately displayed on the pedestal waveform.

5.2 RELATIVE BEAM INTENSITIES USED TO FORM THE INTERFERENCE FRINGES

The condition for least possible error in a visibility measurement occurs when the beam intensities are equal. However, it may be shown that for observations that satisfy Eqs. (5a and b) and for paraxial observations, the beams may be mismatched in intensity by 30 percent and still produce visibility errors of 1 percent or less.

5.3 RELATIVE COHERENCE OF THE BEAMS

With currently available lasers and path-matched beam splitting techniques this parameter does not appear to present any significant problem.

5.4 PHOTON–LIMITED SIGNALS

Photon-limited signals will occur when insufficient light is scattered to the detector. This condition exists when the signal-to-noise ratio becomes less than a specified value which is determined by acceptable error limitations in the measurement process. Generally speaking, photon limited signals can be minimized by carefully designing the interferometer system.

5.5 RADIATION PRESSURE EFFECTS ON VERY SMALL PARTICLES

Gaussian laser beams may be used to contain small particles and to levitate them through a true radiation pressure phenomenon. Such effects have been demonstrated on nearly stationary spheres. However, for moving particles, a momentum calculation will show that a 0.1-μm-diam particle moving 1 cm/sec, illuminated by a 1-mw beam 100 μm in diameter, will be deviated off a straight trajectory normal to the beam by less than 0.3°. Therefore, the probability of the laser beam measurably affecting the particles would appear to be exceptionally small.

5.6 LIGHT ABSORPTION BY THE PARTICLES

These phenomena can be fitted into the general category of particle index of refraction effects. For paraxial observations these effects

have been shown to be negligible, both analytically and experimentally. When the particle is highly absorbing and large, then reflection effects discussed elsewhere can radically change the value of the visibility observed nonparaxially and, therefore, the particle size cannot be determined from the visibility without additional information such as a signal magnitude.

5.7 INDEX OF REFRACTION OF MEDIUM SURROUNDING THE PARTICLES

The index of refraction of the medium affects the position of the probe volume and the value of the fringe period. Equation (1) indicates that as the index of refraction varies, the value of the fringe period changes. Index of refraction values for gases are unity out to four or five decimal places so that the magnitude of the change over a short path is usually insignificant. However, changes in index of refraction also affect the relative phases of the wavefronts in the probe volume and thereby shift the spatial position of the interference fringes while leaving the value of the fringe period unchanged. Thus, attempts to associate phase of the signal with particle size appears impractical since the visibility can produce ambiguous values of D/δ.

A vast body of literature exists on the effects of a medium with random inhomogeneities in the density (which is related directly to the index of refraction for dielectric media) on electromagnetic wave propagation. This literature shows that when the light must propagate through a highly turbulent medium the above effects plus scintillation of the intensity and beam wander occur. These effects diminish with increasing optical wavelengths. Furthermore, these effects occur as time average phenomena over time scales which are long compared to the times usually associated with a visibility and velocity measurement. Investigators have shown that in these cases good quality data can be taken. However, the circumstances under which the data will be limited for essentially instantaneous measurements is not known. Considerable further study is required in this area.

5.8 LIMITING PARTICLE SIZE (MAXIMUM AND MINIMUM)

This parameter is a function of the shape of the particle, and only spherical particles will be considered. Extension to other shapes requires additional analysis along similar lines. For a constant fringe spacing, δ, the particle size limit determined by an accuracy limit of

±1 percent places a lower size limit of 0.1 δ on the particle diameter while the upper limit is restricted by the fact that small values of the visibility can be associated with many values of D/δ. The anomaly is removed by restricting the upper particle size to be less than or equal to one fringe period. With these restrictions, the theoretical lower limit in particle size measurement is about 0.05 wavelengths of the illuminating laser line. The upper size limit is dictated by practical limitations, such as beam splitting techniques, to about a millimeter. A further size restriction is placed by the optical system. If the optical system must be self-aligning, then a lower limit on particle size determination is about 0.5 wavelengths of the illumination.

Extreme difficulties were encountered when attempting to make visibility measurements of particles whose sizes were below 5.0 μm (see Section 3.4). Additional refinements in the control of the experiments are required. Nevertheless, it has been established that particle sizes on the order of 0.5 μm can be measured utilizing this technique. Unfortunately, time did not permit further experiments to be performed to substantiate the lower limit (0.05 λ_o). Additional work is required to determine the threshold of particle size detection, particularly under dynamic operating conditions.

5.9 PARTICLE SHAPE EFFECTS

The visibility is a direct function of particle shape, and the shape must be known or assumed in order to determine size from a one-component visibility measurement. This is not an uncommon feature for all object size determinations from scattered light measurements. The problem of determining the size of odd shaped particles appears to be a universal one since there is no commonly accepted size parameter. Until a suitable size standard can be set for odd shaped particles it would seem that the most straightforward solution to the dilemma is to use a two-dimensional set of interference fringes (i.e., two independent fringe sets sharing a common probe volume with the respective fringe planes orthogonal to each other) to determine relative symmetry properties of the particle. For example, if both measured visibilities are identical, then the particle shape is assumed to be square or circular. Since square shapes do not occur frequently in most natural processes, the particle presumably was spherical in shape. On the other hand, when the visibility is not the same for each signal, cylindrical or ellipsoidal symmetry could be assumed and the major and minor dimensions of the particle specified.

5.10 MULTIPLE PARTICLE SIGNALS

In order to analyze multiple particle signals, at least 80 particles should exist in the probe volume at any instant in time in order for Eq. (16) to be a valid approximation. Fewer than 30 particles can lead to significant deviations from those predicted by this equation, and even for this number certain rare spatial positions of the particles can lead to surprisingly large deviations. No straightforward means has yet been developed to determine non-mono-disperse size distributions from visibility measurements. For practical applications, multiple particle considerations will be an academic exercise. Experimental experience has shown that when a medium containing the particles is optically thin, the probability of observing more than one particle during a signal cycle is very small. Thus, particle size distributions can be determined by measurement of individual particles and forming histograms of number versus size as determined by visibility measurements.

6.0 RECOMMENDATIONS

From the analysis that has been reported here, one conclusion is that the fringe visibility technique can be incorporated into a viable instrument for the real time analysis of particle sizes simultaneously with velocity measurements. Particle sizes to 1.0 μm can be determined; however, the threshold of detection has not been established. For self-aligning optics, 0.5 wavelengths of the illuminating beam appears to be the limit, e.g., in the case of the He-Cd laser, operating at 4416 Å, approximately 0.22 μm. With the laser operating at 3250 Å, then the threshold would be further lowered to approximately 0.17 μm. Additional experimental effort is required to substantiate these conclusions.

One-dimensional particle sizing experiments leave much to be desired. Two-dimensional particle sizing is a minimum condition for realizing reliable measurements. Thus, additional experiments with a two-dimensional fringe technique are recommended to be performed. The experiments should be designed to focus on particle sizes below 1.0 μm. After preliminary static measurements are made and microscopic photographs are obtained for the particle size, then dynamic measurements should be made to ascertain the validity of the theoretical predictions made during this phase of the study.

A newly developed telescope system (Ref. 17), where it will be possible to acquire not only two-dimensional fringe visibilities but where two wavelengths, e.g., 4416 Å and 3250 Å can be used simultaneously, is recommended for further studies. In this manner, a correlation between the two sets of data on the same particulates being measured can be performed to verify the accuracy of the technique.

An electronic device to automatically determine signal visibility is an absolute necessity for on-line particle sizing measurements. Preliminary studies conducted during this effort indicate the feasibility of developing such an instrument.

Upon completion of the prototype subsystems the instrumentation system should be checked out initially in a controlled environment and then used in established, practical, test systems to determine (1) the quality, accuracy, and data acquisition rate as a function of signal-to-noise relationships, (2) additional refinements to be incorporated into the system to make it an operational tool, and (3) determination of operational details, e.g., sampling methods, data analysis and evaluation, correlation with sampling probes or other measuring techniques.

REFERENCES

1. Davies, R. "Rapid Response Instrumentation for Particle Size Analyses." A Series of Review Articles in American Laboratory, Vol. 5, No. 12, December 1973; Vol. 6, No. 1, January 1974; and Vol. 6, No. 2, February 1974.

2. Trollinger, J. D. and Belz, R. A. "Holography in Dust Erosion Facilities." AEDC-TR-73-160 (AD766420), September 1973.

3. Belz, R. A. and Dougherty, N. S. "In-Line Holography of Reacting Liquid Sprays." Proceedings of the Symposium on Engineering Methods of Holography. Sponsored by ARPA, Conducted by TRW Systems, Los Angeles, California, February 1972.

4. Wuerker, R. F. "Applications of Pulsed Laser Holography." Published in Laser Technology in Aerodynamic Measurements, AGARD-LS-49, p. 8.1, 1972.

5. Lennert, A. E., Hornkohl, J. O., and Kalb, H. T. "The Application of Laser Velocimeters for Flow Measurements." Published in The Air Breathing Propulsion Conference Proceedings, Monterey, California, September 19-21, 1972.

6. Brayton, D. B., Kalb, H. T., and Crosswy, F. L. "Two-Component, Dual-Scatter, Laser Doppler Velocimeter with Frequency Burst Signal Readout." Applied Optics, Vol. 12, No. 6, June 1973.

7. Kalb, H. T., Brayton, D. B., and McClure, J. A. "Laser Velocimetry Data Processing." AEDC-TR-73-116 (AD766418), September 1973.

8. Rudd, M. J. "A New Theoretical Model for the Laser Doppler Meter." Journal of Scientific Instruments (Journal of Physics E), Series 2, Vol. 2, 1969.

9. Farmer, W. M. "Measurement of Particle Size, Number Density and Velocity Using a Laser Interferometer." Applied Optics, Vol. 11, No. 11, November 1972.

10. Kerker, M. The Scattering of Light. Academic Press, New York, 1969.

11. Farmer, W. M. "The Interferometric Observation of Dynamic Particle Size, Velocity, and Number Density." Ph. D. Thesis, College of Liberal Arts, Department of Physics, The University of Tennessee, Knoxville, Tennessee, March 1973.

12. Born, M. and Wolf, E. Principles of Optics. Third Edition, Pergamon Press, New York, 1965.

13. Farmer, W. M. and Brayton, D. B. "Analysis of Atmospheric Laser Doppler Velocimeters." Applied Optics, Vol. 10, No. 10, October 1971.

14. Beers, Y. Introduction to the Theory of Error. Addison-Wesley Publishing Company, Inc., Reading, Massachusetts, 1957.

15. Brayton, D. B. and Goethert, W. H. "A New Dual-Scatter Laser Doppler-Shift Velocity Measuring Technique." ISA Transactions, Vol. 10, No. 1, January 1971.

16. Farmer, W. M. and Hornkohl, J. O. "Two-Component Self-Aligning Laser Vector Velocimeter." Applied Optics, Vol. 12, No. 11, November 1973.

17. Lennert, A. E., Crosswy, F. L., Kalb, H. T., et al. "Application of the Laser Velocimeter for Trailing Vortex Measurements." AEDC-TR-74-26 (ADA002151), December 1974.